J. Fluid Mech. (2003), *vol.* 483, *pp.* 37–65. © 2003 Cambridge University Press
DOI: 10.1017/S0022112003004105 Printed in the United Kingdom

Variational methods and maximal residual wall layers

By I. A. FRIGAARD[1,2]†, S. LEIMGRUBER[3] AND O. SCHERZER[3]

[1]Department of Mathematics, University of British Columbia, 1984 Mathematics Road, Vancouver, BC, V6T 1Z2, Canada

[2]Department of Mechanical Engineering, University of British Columbia, 2324 Main Mall, Vancouver, BC, V6T 1Z4, Canada

[3]Department of Computer Science, University of Innsbruck, Technikerstrasse 25, A-6020 Innsbruck, Austria

(Received 26 March 2002 and in revised form 16 November 2002)

The problem of removing an unyielded visco-plastic material from the walls of a duct is considered. This forms a prototype problem for the mechanical removal of soft solids from the duct walls in both oilfield well construction and food processing.

We consider two-layer axial flows for which both fluids may be characterized as Herschel–Bulkley fluids, a class of fluids including Newtonian, Bingham and power-law models. If the yield stress of the displaced fluid is sufficiently large, it is possible for static layers of fluid to persist at the walls of the duct, as has been shown in Allouche, Frigaard & Sona (2000). Following Prager (1954) two variational principles are derived for these flows. These may be loosely interpreted as rate-of-strain minimization and stress maximization principles. The rate-of-strain minimization principle leads directly to existence and uniqueness results for this class of flows. The stress maximization principle leads to a number of qualitative results. An adaptation of the stress maximization principle also allows us to define the concept of a maximal static wall layer in terms of minimization of a certain functional over the space of admissible fluid–fluid interfaces, i.e. a shape optimization problem. We present a number of geometrically simple examples that demonstrate the validity of this method.

1. Introduction

There are many applications in which an attempt is made to remove material from a duct by pumping a fluid through the duct. The following are examples.

(*a*) In the food industry soft solids often form on the walls of processing machinery (due for example to thermal-instability-related fouling), and must be regularly cleaned off, e.g. Changani, Belmar-Beiny & Fryer (1997); Plett (1985).

(*b*) In the preparation of beef for human consumption, the recent emergence of Bovine Spongiform Encephalopathy (BSE) has led to increased vigilance in removal of material from the spinal cavity. This is achieved by pumping a fluid through the spinal duct.

† Author to whom correspondence should be addressed.

https://doi.org/10.1017/S0022112003004105 Published online by Cambridge University Press

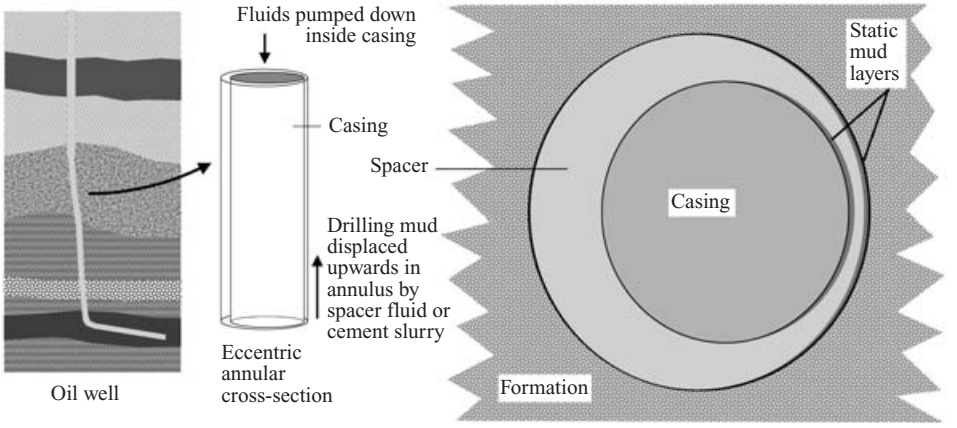


FIGURE 1. Primary cementing of an oil well. Fluid–fluid displacement in a narrow eccentric annulus. Static residual mud layers.

(*c*) In primary cementing of an oil well, removal of the drilling mud from the annular space between the casing and rock formation is attempted by displacing it with fluids. The drilling mud has a yield stress and may remain stuck to the walls or even bridge the gap between the inner and outer walls of the annulus; see for example: McLean, Manry & Whitaker (1966), Jamot (1974), Beirute (1977), Lockyear & Hibbert (1989), Lockyear, Ryan & Gunningham (1989), Couturier *et al.* (1990), Ravi & Beirute (1992), Allouche, Frigaard & Sona (2000), Frigaard, Scherzer & Sona (2001), Bittleston, Ferguson & Frigaard (2002).

In each application it is necessary to distinguish between mechanical and non-mechanical cleaning/removal mechanisms. The latter usually involve a combination of diffusive and reactive processes, e.g. the use of a chemical surfactant. Here we consider purely mechanical removal. We also focus on those applications where the residual wall layer of *in situ* material is wholly static due to the presence of a yield stress in this material. Thus, the material to be displaced will be modelled as a visco-plastic fluid (although its behaviour when yielded is not of direct concern).

In the discussion of mechanical removal it is also necessary to distinguish between laminar and turbulent removal. In the first application mentioned above it is common to use a turbulent cleaning fluid, since machinery duct walls are robust. In the second application, laminar cleaning may be preferable in order to minimize spillage. In the primary cementing application there are many situations in which, for operational reasons, the displacing fluids are not pumped in the turbulent flow regime. Instead one is forced to exploit rheological and density effects to remove the drilling mud in a laminar displacement, e.g. Couturier *et al.* (1990), Allouche *et al.* (2000), Frigaard *et al.* (2001), Bittleston *et al.* (2002).

In this paper we concentrate on primary cementing displacements. In this process a sequence of fluids is pumped through a narrow eccentric annulus in an effort to displace the drilling mud, see figure 1. The annular gap is formed by the outside wall of the steel casing and the inside wall of the drilled rock formation. When the operation is performed in the laminar flow regime, the displacing fluid is typically either a spacer fluid or is the leading cement slurry. Both these fluids and the drilling mud are typically visco-plastic and shear-thinning (for further process details see Guillot *et al.* 1990; Smith 1987). Significant problems can occur if static residual layers of drilling

https://doi.org/10.1017/S0022112003004105 Published online by Cambridge University Press

mud remain on the walls of the annulus. The process of cement setting is strongly exothermic and also hydrophilic. Thus, water is extracted from the mud layers as the cement sets (even in the case of an oil-based mud, which still contains significant water fraction). After setting the mud layers are typically much more permeable than the set cement and can extend axially along the annulus connecting different fluid-bearing regions of the rock formation. The so-called *wet micro-annulus* that is created destroys the zonal isolation of the well and the consequent pressure drop in the oil reservoir can severely damage the productivity of the well; see Economides (1990). Eliminating the occurrence of static residual wall layers forms the motivation for this study.

A number of researchers have analysed the axial flow of visco-plastic fluids in an eccentric annulus; see for example Szabo & Hassager (1992); Walton & Bittleston (1991). However, these studies are confined to flows of a single fluid. A fairly extensive study of the displacement of a visco-plastic fluid by a second miscible fluid (visco-plastic or otherwise) has been recently carried out in Allouche *et al.* (2000), Frigaard *et al.* (2001), Gabard-Cuoq (2001) and Frigaard, Allouche & Gabard-Cuoq (2001). These studies focus mainly on iso-density displacements in a plane channel and in a pipe. They specifically study the situation in which the yield stress of the displaced fluid is larger than that of the displacing fluid and a near uniform static residual layer is left on the walls of the duct, while a symmetric finger of the displacing fluid steadily propagates along the centre of the duct. These studies have been largely successful in giving a prediction of the thickness of the residual layer, by a fairly simple calculation, see Allouche *et al.* (2000). However, such studies only begin to touch the surface of a fascinating and complex non-Newtonian displacement process. If the duct is inclined and a density difference is introduced (as in the cementing process) the symmetry of the displacement is broken and many new phenomena can arise.

In this paper we avoid these complexities. Instead of trying to predict the actual layer thickness we concentrate on predicting the maximal static residual layer thickness in a duct. Although from Allouche *et al.* (2000) and Gabard-Cuoq (2001) it is known that the maximal layer gives a conservative prediction of the actual layer thickness, there are significant advantages to the approach we adopt. First, if the maximal static layer is zero, there is no residual layer and the displacement process is definitively effective, i.e. good. Secondly, there is a significant reduction in terms of the number of dimensionless parameters that must be considered and a significant simplification in the field equations that define the underlying flow. Thirdly, this approach leads us to a general formulation of the computational problem that will allow the investigation of complex duct geometries (although here we present only geometrically simple examples).

The underlying approach is as follows. We characterize our fluids, both displaced and displacing, as Herschel–Bulkley fluids, which incorporates Newtonian, Bingham and power-law fluid models as simplifications. We consider a displacement of one Herschel–Bulkley fluid by another miscible fluid along a long duct at a fixed flow rate. The displaced fluid (mud) is assumed to have a larger yield stress than the displacing fluid (cement slurry or spacer), which need not have a yield stress. We assume that there is a fully three-dimensional flow only in a region close to the displacement front. This region advances along the duct as the displacement continues. We ignore the three-dimensional flow and consider instead a region far behind the displacement front. Here we assume that the flow has become (near) axial.

We consider a cross-section of the duct somewhere in the axial flow region and suppose that there is a residual mud layer attached to the walls, see figure 1. We

https://doi.org/10.1017/S0022112003004105 Published online by Cambridge University Press

address the question of what is the maximal mud wall layer that can remain static for a given imposed flow rate and fluid properties. That such a maximal layer exists is physically obvious, at least in simply connected regions (in § 3.1 we also sketch a mathematical proof). For example, consider a pipe with a static mud layer on the wall. A fixed flow rate is pumped through the pipe. If the wall layer grows and remains static, it constricts the cross-section through which the displacing fluid passes. The pressure drop required to achieve this flow rate increases and hence also the shear stress in the fluid. Eventually, this shear stress will exceed the yield stress of the mud layer and it will start to flow.

Although our focus is on maximal static residual wall layers, these flows form part of a wider class of flows, namely axial flows of multiple Herschel–Bulkley fluids, which have other applications. For example, plug cementing flows of Bingham fluids have been considered in Fenie & Frigaard (1999); Frigaard (1998); Frigaard & Crawshaw (1999), and much of the background theory for Bingham fluids is developed in Frigaard & Scherzer (1998, 2000). Recently, it has also been shown that certain multi-layer flow configurations in which a visco-plastic fluid is used as the lubricating wall layer (i.e. flowing and not static, as here), lead to the elimination of interfacial instabilities (see Frigaard 2001), which hamper the use of multi-layer viscous flows in many industrial contexts. This direction is also being actively researched. Thus, in the first part of this paper we consider axial flows of multiple Herschel–Bulkley fluids in slightly more generality than is needed later, establishing existence and uniqueness results for weak solutions and developing variational principles, which are used later. Our variational principles are based on the work of Prager (1954) and Duvaut & Lions (1976) for Bingham fluids, which have been extended to slow flows of a single Herschel–Bulkley fluid in Zwick, Ayyaswamy & Cohen (1996) and Huilgol (1998); see also Huilgol & Nguyen (2001).

An outline of the paper is as follows. In § 2 we present a mathematical description of axial flows of multiple Herschel–Bulkley fluids and derive general results. In § 3 we explain the concept of a maximal static wall layer, derive elementary properties and formulate a rigorous definition of the maximal wall layer in terms of a shape optimization problem. Section 4 presents the results of test computations in slot and concentric annular geometries. Whilst avoiding geometric complexity, we are able to verify the feasibility of the general approach. The paper concludes with a discussion.

2. Axial multi-fluid flows

Our aim in the following sections is to establish the basic properties of axial flows of multiple Herschel–Bulkley fluids, i.e. can we find solutions, how do these solutions depend on the problem parameters, etc. This establishes the foundation for § 3, where we consider how to find the solution that maximizes the residual wall layers. Much of §§ 2.1–2.4 may be skipped at first reading by a reader not interested in the mathematical detail. In § 2.5 we give a more physical interpretation of our results on these flows.

We consider a flow domain Ω that represents the cross-section of a duct. The domain is divided into a countable number of sub-domains, in each of which one of two fluids is present, which we shall distinguish by the subscripts s and m. The union of the sub-domains of each fluid is denoted $\Omega_k : k = s, m$. The superscript m denotes the drilling mud and the superscript s denotes a cement slurry or spacer fluid. It is assumed that each sub-domain has a Lipschitz continuous boundary. The flow is assumed axial with dimensionless axial velocity denoted $w(x, y)$. The z-axis aligns

https://doi.org/10.1017/S0022112003004105 Published online by Cambridge University Press

with the direction of the flow (also the duct axis). The velocity $w(x, y)$ is determined by the following field equations, which may be derived straightforwardly from the Navier–Stokes equations using scaling arguments (for example, as in Frigaard & Scherzer 1998):

$$\frac{\partial}{\partial x}\tau_{m,zx} + \frac{\partial}{\partial y}\tau_{m,zy} = -f, \qquad (x, y) \in \Omega_m, \tag{2.1}$$

$$\frac{\partial}{\partial x}\tau_{s,zx} + \frac{\partial}{\partial y}\tau_{s,zy} = b - f, \qquad (x, y) \in \Omega_s. \tag{2.2}$$

Here f is the modified pressure gradient and b is a buoyancy parameter. The shear stresses $\tau_{k,zj}$ are defined for $k = s, m;\ j = x, y$ by

$$\tau_k > \tau_{k,Y} \Longleftrightarrow \boldsymbol{\tau}_k = (\tau_{k,zx}, \tau_{k,zy}) = \left[\kappa_k |\nabla w|^{n_k - 1} + \frac{\tau_{k,Y}}{|\nabla w|}\right] \nabla w \tag{2.3}$$

$$|\nabla w| = 0 \Longleftrightarrow \tau_k \leqslant \tau_{k,Y}, \tag{2.4}$$

with

$$\tau_k \equiv \left[\tau_{k,zx}^2 + \tau_{k,zy}^2\right]^{1/2}. \tag{2.5}$$

The constants κ_k, n_k, $\tau_{k,Y}$, $k = s, m$ are respectively the consistency, power-law index and yield stress of each fluid.

The domain Ω is bounded (in the mathematical sense), with boundary denoted $\partial\Omega$, on which

$$w(x, y) = 0. \tag{2.6}$$

Physically, $\partial\Omega$ represents the closed wall of the duct cross-section Ω. The interface between spacer and mud regions is denoted by Γ with normal vector $\boldsymbol{n} = (n_x, n_y)$ defined a.e. on Γ. On Γ the following conditions are satisfied:

$$\boldsymbol{\tau}_m \cdot \boldsymbol{n} = \boldsymbol{\tau}_s \cdot \boldsymbol{n}, \tag{2.7}$$

$$w(x, y) \quad \text{continuous.} \tag{2.8}$$

Equations (2.1)–(2.8) constitute the classical statement of this problem.

Relation to dimensionless parameters

In deriving (2.1)–(2.8) lengths have been scaled with $\hat{R}$, characteristic of the duct cross-section. The velocity scale is denoted $\hat{U}_0$, which we will define later. All stresses are scaled with $\hat{\rho}^{[m]}\hat{U}_0^2$, where $\hat{\rho}^{[m]}$ is the mud density. The modified pressure gradient f and the buoyancy parameter b are

$$f = -\frac{\mathrm{d}p}{\mathrm{d}x} - \frac{\hat{U}_0^2}{\hat{g}\hat{R}}, \qquad b = \frac{\hat{U}_0^2}{\hat{g}\hat{R}}\left[\frac{\hat{\rho}^{[s]} - \hat{\rho}^{[m]}}{\hat{\rho}^{[m]}}\right], \tag{2.9}$$

where $\hat{g}$ is the gravitational acceleration and $\hat{\rho}^{[s]}$ is the spacer density. Dimensionless rheological parameters are defined in terms of their dimensional equivalents by

$$\kappa_k = \frac{\hat{\kappa}_k \hat{U}_0^{n_k - 2}}{\hat{\rho}^{[m]}\hat{R}^{n_k}}, \qquad \tau_{k,Y} = \frac{\hat{\tau}_{k,Y}}{\hat{\rho}^{[m]}\hat{U}_0^2}. \tag{2.10}$$

2.1. *Rate of strain minimization*

If w is a classical solution of (2.1)–(2.8), it can be straightforwardly shown that:

$$a(w, v - w) + j(v) - j(w) \geqslant L(f, v - w), \quad \forall v \in C_0^\infty(\Omega), \tag{2.11}$$

https://doi.org/10.1017/S0022112003004105 Published online by Cambridge University Press

where

$$a(w, v) = \kappa_s a_s(w, v) + \kappa_m a_m(w, v)$$
$$\equiv \kappa_s \int_{\Omega_s} |\nabla w|^{n_s - 1} \nabla w \cdot \nabla v \, \mathrm{d}\Omega + \kappa_m \int_{\Omega_m} |\nabla w|^{n_m - 1} \nabla w \cdot \nabla v \, \mathrm{d}\Omega, \tag{2.12}$$

$$j(v) = \tau_{s,Y} j_s(v) + \tau_{m,Y} j_m(v) \equiv \tau_{s,Y} \int_{\Omega_s} |\nabla v| \, \mathrm{d}\Omega + \tau_{m,Y} \int_{\Omega_m} |\nabla v| \, \mathrm{d}\Omega, \tag{2.13}$$

$$L(f, v) \equiv (f - b) \int_{\Omega_s} v \, \mathrm{d}\Omega + f \int_{\Omega_m} v \, \mathrm{d}\Omega. \tag{2.14}$$

See for example Huilgol (1998) for a detailed derivation of this inequality. We define $p = 1 + \min\{n_m, n_s\}$ and consider the space $V = W_0^{1,p}(\Omega)$, the closure of $C_0^\infty(\Omega)$ with respect to the norm:

$$\|v\|_{W^{1,p}(\Omega)} = \left[\int_\Omega |\nabla v|^p + |v|^p \, \mathrm{d}\Omega \right]^{1/p}.$$

We take

$$a(w, v - w) + j(v) - j(w) \geqslant L(f, v - w), \quad w \in V, \forall v \in V, \tag{2.15}$$

as the weak definition of (2.1)–(2.8). A solution to (2.15) will also satisfy the following minimization problem:

$$\inf_{v \in V} J(v) : \quad J(v) \equiv \frac{\kappa_s}{n_s + 1} a_s(v, v) + \frac{\kappa_m}{n_m + 1} a_m(v, v) + j(v) - L(f, v). \tag{2.16}$$

The minimization principle (2.16) has been derived for the slow flow of a single Herschel–Bulkley fluid in Zwick *et al.* (1996) and Huilgol (1998). These derivations are quite detailed and may be of independent interest to the reader. The principal difference here to the above-mentioned work is our consideration of multiple fluids. Our reliance on functional analytic methods, allows us to use (2.16) straightforwardly to establish the existence of a weak solution.

We note that $J(v)$ is proper, strictly convex and that $J(v) \to \infty$ as $\|v\|_{W^{1,p}(\Omega)} \to \infty$, since the semi-norm $\int_\Omega |\nabla v|^p \, \mathrm{d}\Omega$ is an equivalent norm to $\|v\|_{W^{1,p}(\Omega)}$ on $W_0^{1,p}(\Omega)$; see for example Atkinson & Han (2001, § 6.3.5), or Dacoragna (1989). Hence, by standard methods from convex analysis, see Glowinski (1983, chap. 5), there exists a unique solution $w \in V = W_0^{1,p}(\Omega)$ to (2.16), which also satisfies (2.15). Finally, we note that by using the trial functions $v = 0,\ 2w$ in (2.15) and combining the inequalities, we see that the solution w satisfies

$$a(w, w) + j(w) - L(f, w) = 0,$$

and hence

$$J(w) = -\frac{n_s}{n_s + 1} \kappa_s a_s(w, w) - \frac{n_m}{n_m + 1} \kappa_m a_m(w, w), \tag{2.17}$$

which is used later.

2.2. *Stress maximization*

The rate of strain minimization (2.16) is relatively well known for Bingham fluids, see e.g. Prager (1954), Duvaut & Lions (1976) and Glowinski (1983). The flows which we study also satisfy a second variational principle, in which a certain functional of the stress is maximized. The stress maximization principle was first derived by Prager for slow flows of a Bingham fluid and has been extended to the Herschel–Bulkley fluid by

https://doi.org/10.1017/S0022112003004105 Published online by Cambridge University Press

Zwick *et al.* (1996); see also Huilgol (1998). Here we consider multi-fluid flows. Apart from our extension to multi-fluids, the principle that we state is analogous to that of Zwick *et al.* (1996), who adapt the earlier work of Yoshioka & Adachi (1971*a*, *b*).

We suppose a given partition of Ω into Ω_s and Ω_m. We consider a triple $(\tilde{f}, \tilde{\tau}_x, \tilde{\tau}_y)$ such that

$$\tilde{f} \text{ constant}, \quad \tilde{\boldsymbol{\tau}} = (\tilde{\tau}_x, \tilde{\tau}_y) \in [C^1(\Omega_s) \cap C^1(\Omega_m)]^2.$$

We say that the triple $(\tilde{f}, \tilde{\tau}_x, \tilde{\tau}_y)$ is admissible if

$$\nabla \cdot \tilde{\boldsymbol{\tau}} = -\tilde{f}, \qquad (x, y) \in \Omega_m, \tag{2.18}$$

$$\nabla \cdot \tilde{\boldsymbol{\tau}} = b - \tilde{f}, \qquad (x, y) \in \Omega_s. \tag{2.19}$$

$$\tilde{\boldsymbol{\tau}} \cdot \boldsymbol{n} \quad \text{continuous on } \Gamma, \tag{2.20}$$

and denote by S_Γ the set of admissible $(\tilde{f}, \tilde{\tau}_x, \tilde{\tau}_y)$.

THEOREM 1. *Let w solve the classical problem* (2.1)–(2.8). *Then the triple* $(f, \tau_{zx}, \tau_{zy}) \in S_\Gamma$ *and* $(f, \tau_{zx}, \tau_{zy})$ *maximizes the functional* $F(\tilde{\boldsymbol{\tau}}, \tilde{f})$:

$$\begin{aligned} F(\tilde{\boldsymbol{\tau}}, \tilde{f}) \equiv (\tilde{f} - b) \int_{\Omega_s} w \, \mathrm{d}\Omega + \tilde{f} \int_{\Omega_m} w \, \mathrm{d}\Omega \\ - \frac{n_s}{n_s + 1} \frac{1}{\kappa_s^{1/n_s} 2^{1+1/n_s}} \int_{\Omega_s} (|\tilde{\tau} - \tau_{s,Y}| + \tilde{\tau} - \tau_{s,Y})^{1+1/n_s} \, \mathrm{d}\Omega \\ - \frac{n_m}{n_m + 1} \frac{1}{\kappa_m^{1/n_m} 2^{1+1/n_m}} \int_{\Omega_m} (|\tilde{\tau} - \tau_{m,Y}| + \tilde{\tau} - \tau_{m,Y})^{1+1/n_m} \, \mathrm{d}\Omega \end{aligned} \tag{2.21}$$

over S_Γ, where $\tilde{\tau} = |\tilde{\boldsymbol{\tau}}|$.

Proof. See the Appendix.

2.3. *Relationship between* (2.16) *and* (2.21)

Whilst (2.16) and (2.21) are not strictly equivalent, the relationship between them is quite easily established, at least formally, as we will show in the following. Assuming the existence of a maximizer to (2.21) we relax (2.18) and (2.19) by introducing a multiplier:

$$\max_{(\tilde{\boldsymbol{\tau}}, \tilde{f}) \in S_\Gamma} F(\tilde{\boldsymbol{\tau}}, \tilde{f}) = \max_{(\tilde{\boldsymbol{\tau}}, \tilde{f})} \min_{\lambda} \left\{ F(\tilde{\boldsymbol{\tau}}, \tilde{f}) - \int_{\Omega_m} \lambda (\nabla \cdot \tilde{\boldsymbol{\tau}} + \tilde{f}) \, \mathrm{d}\Omega - \int_{\Omega_s} \lambda (\nabla \cdot \tilde{\boldsymbol{\tau}} + \tilde{f} - b) \, \mathrm{d}\Omega \right\} \tag{2.22}$$

where $\lambda \in C_0^0(\Omega) \cap C^1(\Omega_m) \cap C^1(\Omega_s)$. This is the standard way of solving a constrained optimization problem, see e.g. Quarteroni, Sacco & Saleri (2000). Using the divergence theorem and (2.20) we obtain

$$\max_{(\tilde{\boldsymbol{\tau}}, \tilde{f})} \min_{\lambda} \left\{ F(\tilde{\boldsymbol{\tau}}, \tilde{f}) + \int_{\Omega_m} \tilde{\boldsymbol{\tau}} \cdot \nabla \lambda - \lambda \tilde{f} \, \mathrm{d}\Omega + \int_{\Omega_s} \tilde{\boldsymbol{\tau}} \cdot \nabla \lambda - \lambda (\tilde{f} - b) \, \mathrm{d}\Omega \right\}. \tag{2.23}$$

The optimality condition with respect to $\tilde{\boldsymbol{\tau}}$ gives for all $\tilde{\boldsymbol{h}}$:

$$\begin{aligned} 0 = \int_{\Omega_m | \tau_m \leqslant \tau_{m,Y}} \tilde{\boldsymbol{h}} \cdot \nabla \lambda \, \mathrm{d}\Omega + \int_{\Omega_m | \tau_m > \tau_{m,Y}} \tilde{\boldsymbol{h}} \cdot \left[\nabla \lambda - \frac{(\tau_m - \tau_{m,Y})^{1/n_m}}{\kappa_m^{1/n_m}} \frac{\boldsymbol{\tau}_m}{\tau_m} \right] \mathrm{d}\Omega \\ + \int_{\Omega_s | \tau_s \leqslant \tau_{s,Y}} \tilde{\boldsymbol{h}} \cdot \nabla \lambda \, \mathrm{d}\Omega + \int_{\Omega_s | \tau_s > \tau_{s,Y}} \tilde{\boldsymbol{h}} \cdot \left[\nabla \lambda - \frac{(\tau_s - \tau_{s,Y})^{1/n_s}}{\kappa_s^{1/n_s}} \frac{\boldsymbol{\tau}_s}{\tau_s} \right] \mathrm{d}\Omega \end{aligned}$$

https://doi.org/10.1017/S0022112003004105 Published online by Cambridge University Press

so that

$$\tau_k > \tau_{k,Y} \Longleftrightarrow \boldsymbol{\tau}_k = \nabla\lambda = \frac{(\tau_k - \tau_{k,Y})^{1/n_k}}{\kappa_k^{1/n_k}} \frac{\boldsymbol{\tau}_k}{\tau_k} \equiv \left[\kappa_k |\nabla\lambda|^{n_k - 1} + \frac{\tau_{k,Y}}{|\nabla\lambda|}\right] \nabla\lambda,$$

$$|\nabla\lambda| = 0 \Longleftrightarrow \tau_k \leqslant \tau_{k,Y},$$

Substituting in (2.23) we obtain

$$\max_{\tilde{f}} \min_{\lambda} \left\{ \tilde{f} \int_{\Omega_m} (w - \lambda)\, \mathrm{d}\Omega + (\tilde{f} - b) \int_{\Omega_s} (w - \lambda)\, \mathrm{d}\Omega \right.$$
$$s + \frac{1}{1 + n_m} \kappa_m \int_{\Omega_m} |\nabla\lambda|^{1+n_m}\, \mathrm{d}\Omega + \frac{1}{1 + n_s} \kappa_s \int_{\Omega_s} |\nabla\lambda|^{1+n_s}\, \mathrm{d}\Omega$$
$$\left. + \tau_{m,Y} \int_{\Omega_m} |\nabla\lambda|\, \mathrm{d}\Omega + \tau_{s,Y} \int_{\Omega_s} |\nabla\lambda|\, \mathrm{d}\Omega \right\}, \quad (2.24)$$

where the terms multiplying w do not affect the minimizer with respect to λ.

Hence, the minimizer of (2.23) with respect to λ satisfies

$$\min_{\lambda} \left\{ -\tilde{f} \int_{\Omega_m} \lambda\, \mathrm{d}\Omega - (\tilde{f} - b) \int_{\Omega_s} \lambda\, \mathrm{d}\Omega + \frac{1}{1 + n_m} \kappa_m \int_{\Omega_m} |\nabla\lambda|^{1+n_m}\, \mathrm{d}\Omega \right.$$
$$\left. + \frac{1}{1 + n_s} \kappa_s \int_{\Omega_s} |\nabla\lambda|^{1+n_s}\, \mathrm{d}\Omega + j(\lambda) \right\} = \min_{\lambda} J(\lambda). \quad (2.25)$$

Finally, optimality of (2.23) with respect to $\tilde{f}$ gives $\lambda = w$ in (2.25). We note that this relaxation technique could be used to establish the formal equivalence of the variational principles in Zwick *et al.* (1996) and Huilgol (1998).

2.4. *Remarks*

In our later consideration of maximal wall layers we will mainly make use of (2.21). However, for particular applications either (2.16) or (2.21) can prove to be more useful. In passing we outline a number of qualitative results that add to our physical understanding of these flows and that can be derived straightforwardly from either of (2.16) or (2.21).

(*a*) The flow rate $Q(w)$:

$$Q(w) = \int_{\Omega} w\, \mathrm{d}\Omega,$$

increases monotonically with f. To see this, let w_n be the unique solution of (2.16) for $f = f_n$: $n = 1, 2$. Let $F_{w_n}(\tilde{\boldsymbol{\tau}}, \tilde{f})$ be the functional defined by (2.21), with $w = w_n$. Denote the maximizer of $F_{w_n}(\tilde{\boldsymbol{\tau}}$ also by $\tilde{\boldsymbol{\tau}}_n, \tilde{f}_n)$, then

$$0 \leqslant F_{w_1}(\tilde{\boldsymbol{\tau}}_1, \tilde{f}_1) - F_{w_1}(\tilde{\boldsymbol{\tau}}_2, \tilde{f}_2) + F_{w_2}(\tilde{\boldsymbol{\tau}}_2, \tilde{f}_2) - F_{w_2}(\tilde{\boldsymbol{\tau}}_1, \tilde{f}_1),$$
$$= [f_1 - f_2][Q(w_1) - Q(w_2)],$$

establishing monotonicity. On examining the proof of Theorem 1 we see that the inequality will be strict unless $Q(w) = 0$.

(*b*) This monotonicity result means that we are able to either prescribe f and find the solution w, or to prescribe a certain flow rate:

$$Q(w) = Q^*, \quad (2.26)$$

and find the solution (w, f). Note that although w is unique, f need not be in the case $Q^* = 0$. Exchange flows ($Q^* = 0$) have been studied extensively for axial flows

https://doi.org/10.1017/S0022112003004105 Published online by Cambridge University Press

of Bingham fluids in Frigaard (1998), Fenie & Frigaard (1999), Frigaard & Scherzer (1998, 2000) and Frigaard & Crawshaw (1999).

(*c*) The functional $a_k(w, w)$ decreases monotonically with κ_k: $k = s, m$, i.e. if $\kappa_{k,2} \geqslant \kappa_{k,1}$, then

$$a_k(w_1, w_1) \geqslant a_k(w_2, w_2),$$

where w_n is the solution to (2.16) for $\kappa_k = \kappa_{k,n}$: $n = 1, 2$; $k = m, s$. To see this, suppose for example that $\kappa_{s,2} \geqslant \kappa_{s,1}$ and denote by $J_1(v)$ and $J_2(v)$ the functional $J(v)$ in (2.16), with $\kappa_s = \kappa_{s,1}$ and $\kappa_s = \kappa_{s,2}$, respectively, with minimizers w_1 and w_2. Considering $J_2(w_2) - J_1(w_2)$, we observe that

$$J_2(w_2) = \frac{\kappa_{s,2} - \kappa_{s,1}}{n_s + 1} a_s(w_2, w_2) + J_1(w_2) \geqslant \frac{\kappa_{s,2} - \kappa_{s,1}}{n_s + 1} a_s(w_2, w_2) + J_1(w_1),$$

since w_1 is the minimizer of J_1. Therefore, rearranging we have

$$-J_1(w_1) \geqslant \frac{\kappa_{s,2} - \kappa_{s,1}}{n_s + 1} a_s(w_2, w_2) - J_2(w_2).$$

Now considering $J_1(w_1) - J_2(w_1)$ we have

$$J_1(w_1) + \frac{\kappa_{s,2} - \kappa_{s,1}}{n_s + 1} a_s(w_1, w_1) = J_2(w_1) \geqslant J_2(w_2),$$

which, on summing the last two inequalities, gives

$$a_s(w_1, w_1) \geqslant a_s(w_2, w_2).$$

(*d*) Similar comparison methods to (*c*) above also lead to the following results. If $\tau_{k,Y,2} \geqslant \tau_{k,Y,1}$ then

$$\frac{\kappa_s a_s(w_1, w_1)}{1 + 1/n_s} + \frac{\kappa_m a_m(w_1, w_1)}{1 + 1/n_m} \geqslant \frac{\kappa_s a_s(w_2, w_2)}{1 + 1/n_s} + \frac{\kappa_m a_m(w_2, w_2)}{1 + 1/n_m}, \tag{2.27}$$

and

$$j_k(w_1) \geqslant j_k(w_2), \tag{2.28}$$

where w_n is the solution to (2.16) for $\tau_{k,Y} = \tau_{k,Y,n}$: $n = 1, 2$; $k = m, s$.

(*e*) Various results establishing continuity of w with respect to f, $\tau_{k,Y}$ and κ_k can also be established, but have less practical application than the above. The methods are similar to those in Frigaard & Scherzer (1998, 2000), except that the norms are more complex.

2.5. *Physical description*

In § 2.1 we have shown that (for sensible interfaces and physical parameters) we can always find a velocity solution to our multi-fluid problem. The solution lies in $W_0^{1,p}(\Omega)$, which is (loosely speaking) a space of functions satisfying the no-slip conditions on the duct wall and having first partial derivatives defined almost everywhere; the p-exponent refers to the particular norm. Here the fluid with the smallest power-law exponent $n > 0$ determines the space. Obviously, functions in $W_0^{1,p}(\Omega)$ can be more regular than implied by this weak formulation and it is of interest to consider whether this is typically the case, i.e. in a practical situation. In general we must conclude that solutions will not be more regular. In the first place, for a multi-fluid problem we would not expect that the first derivatives will be defined everywhere in Ω, since typically there will be a jump in velocity gradients at an interface where the viscosity changes. Secondly, even if we had identical rheologies (i.e. a single fluid), we

https://doi.org/10.1017/S0022112003004105 Published online by Cambridge University Press

cannot guarantee more regularity. For example, if we examine those simple analytical solutions that can be found for a Herschel–Bulkley fluid, we often find that the solutions are smoother than suggested by $W_0^{1,n+1}(\Omega)$, e.g. in Hagen–Poiseuille flow we have $C^1(\Omega)$ for $n \leqslant 1$ (shear-thinning fluids) and $C^2(\Omega)$ if $n > 1$. However, as the symmetry is broken solutions can become less smooth, see for example the eccentric annular flows in Walton & Bittleston (1991) and particularly the computations in Szabo & Hassager (1992).

Following Zwick *et al.* (1996), one physical interpretation of the two variational principles is that the actual (visco-plastic) dissipation is bounded above and below. Specifically, we can show that

$$F(\tilde{\boldsymbol{\tau}}, \tilde{f}) \leqslant \frac{\kappa_s a_s(w, w)}{1 + 1/n_s} + \frac{\kappa_m a_m(w, w)}{1 + 1/n_m} + j(w) \leqslant J(v) + L(f, w). \tag{2.29}$$

Alternatively, the two principles may be combined to define a total energy functional $T(v, \tilde{\boldsymbol{\tau}}, \tilde{f})$:

$$T(v, \tilde{\boldsymbol{\tau}}, \tilde{f}) = J(v) + L(f, w) - F(\tilde{\boldsymbol{\tau}}, \tilde{f}). \tag{2.30}$$

We see from (2.29) that $T(v, \tilde{\boldsymbol{\tau}}, \tilde{f}) \geqslant 0$ and that for the solution $(w, \boldsymbol{\tau}, f)$ we have $T(w, \boldsymbol{\tau}, f) = 0$. Considering a volume V of the duct, with uniform cross-sectional area Ω, the physical interpretation is that the energy dissipated within V is always greater than the energy flowing into V, for any admissible velocity and stress fields. It is only for the actual velocity and stress that these quantities balance; see Zwick *et al.* (1996).

Regarding our results in § 2.4, it is obviously of interest to know how the solution varies with the different physical parameters. That the flow rate increases with the pressure gradient is intuitive. Practically, in hydraulic applications we often wish to specify the flow rate and not the pressure drop. That we can do so follows from this monotonicity. Also intuitive is the decrease in $a_k(w, w)$ with κ_k. These are flows at a fixed pressure gradient and we expect that the velocity gradient will decrease if the viscosity increases, i.e. it becomes harder to pump the fluid.

The effects of changing the yield stress are less clear. For example, in (2.27) we see that increasing the yield stress in one fluid may decrease the total viscous dissipation in both fluids, i.e. the effect could be non-local. In the case we shall consider below, where the mud layer abuts the wall, increasing the mud yield stress sufficiently will eventually result in a static wall layer. Further increases should then have no effect on the dissipation in either fluid, since the mud layer acts simply as a solid. Hence the decrease is not strictly monotone, either in (2.27) or (2.28).

3. Maximal static wall layers

We now turn to the problem of computing a maximal residual layer of mud. Stated simply, we wish to find the maximal mud domain for which the velocity in the mud is identically zero throughout. This is clearly a problem in shape optimization. In all such problems it is necessary to minimize some functional of the solution, in order to give the optimal shape. Here an apparently natural functional to use is the size of the mud domain $|\Omega_m|$, over which $w = 0$. However, although apparently obvious, this functional involves the mapping of w to the level set $w = 0$. To optimize using only a restricted subset of solution values is intuitively much less stable than doing so using the full set of solution values. For this reason, we seek below a smooth functional that varies monotonically with a nested sequence of mud domains on which $w = 0$. Finding a suitable function is the key result of the paper.

https://doi.org/10.1017/S0022112003004105 Published online by Cambridge University Press

Whereas § 2 has been rather general, we now restrict our attention to partitions of Ω for which each mud sub-domain abuts the duct wall at some point, i.e. we want to consider solutions for which the mud wall layers Ω_m are static. We classify solutions to (2.1)–(2.8) according to the following criteria:

A *general solution*, w, is a classical solution to (2.1)–(2.8), for which f is specified.

A *constrained solution*, (w, f), is a classical solution to (2.1)–(2.8), that satisfies the additional constraint

$$\int_{\Omega} w \, \mathrm{d}\Omega = |\Omega|, \tag{3.1}$$

which arises from choosing the velocity scale $\hat{U}_0$ to be defined by dividing the volumetric flow rate $\hat{Q}$ by the duct cross-sectional area $\hat{A}$. Note that $|\Omega| = \hat{A}/\hat{R}^2$.

A *static wall layer solution*, w, is a classical solution to (2.1)–(2.8), that satisfies the additional constraint

$$w(x, y) = 0, \qquad (x, y) \in \Omega_m, \tag{3.2}$$

i.e. the mud is not moving.

A *constrained static wall layer solution*, w, is a constrained solution to (2.1)–(2.8), that also satisfies (3.2). Note that for a given interface Γ both the general and constrained problems will admit a unique weak solution (see the discussion in § 2.4 for the constrained problem). However, there is clearly no guarantee that a solution will satisfy the additional constraint (3.2).

The principal aim of this section is to formulate the problem of computing the maximal mud domain, Ω_m, that will admit a constrained static wall layer solution.

Remarks

(i) For any constrained solution on Γ the functional $F(\tilde{\boldsymbol{\tau}}, \tilde{f})$, defined by (2.21), is denoted by $F_\Gamma(\tilde{\boldsymbol{\tau}}, f)$ and is given by

$$F_\Gamma(\tilde{\boldsymbol{\tau}}, f) \equiv f|\Omega| - b\int_{\Omega_s} w \, \mathrm{d}\Omega - \frac{n_s}{n_s+1}\frac{1}{\kappa_s^{1/n_s} 2^{1+1/n_s}}\int_{\Omega_s} (|\tilde{\tau} - \tau_{s,Y}| + \tilde{\tau} - \tau_{s,Y})^{1+1/n_s} \, \mathrm{d}\Omega$$
$$- \frac{n_m}{n_m+1}\frac{1}{\kappa_m^{1/n_m} 2^{1+1/n_m}}\int_{\Omega_m} (|\tilde{\tau} - \tau_{m,Y}| + \tilde{\tau} - \tau_{m,Y})^{1+1/n_m} \, \mathrm{d}\Omega. \tag{3.3}$$

(ii) If the interface Γ also admits a constrained static wall layer solution:

$$F_\Gamma(\tilde{\boldsymbol{\tau}}, f) \equiv (f-b)|\Omega| - \frac{n_s}{n_s+1}\frac{1}{\kappa_s^{1/n_s} 2^{1+1/n_s}}\int_{\Omega_s} (|\tilde{\tau} - \tau_{s,Y}| + \tilde{\tau} - \tau_{s,Y})^{1+1/n_s} \, \mathrm{d}\Omega, \tag{3.4}$$

since the mud domain is unyielded and all the fluid passes through Ω_s.

The following is our main result, which we use to define a maximal residual mud layer.

THEOREM 2. *Let (w_1, f_1) be a constrained static mud layer solution for an admissible interface Γ_1 and let (w_2, f_2) be a constrained static mud layer solution for a second admissible interface Γ_2, such that $\Omega_{s,1} \subseteq \Omega_{s,2}$. We have*

$$F_{\Gamma_1}(\boldsymbol{\tau}_1, f_1) \geqslant F_{\Gamma_2}(\boldsymbol{\tau}_2, f_2), \tag{3.5}$$

where $\boldsymbol{\tau}_1$ is the maximizer of $F_{\Gamma_1}(\cdot, f_1)$ and $\boldsymbol{\tau}_2$ is the maximizer of $F_{\Gamma_2}(\cdot, f_2)$.

https://doi.org/10.1017/S0022112003004105 Published online by Cambridge University Press

Proof. From (3.4) and (A 1):

$$\begin{aligned}
F_{\Gamma_1}(\boldsymbol{\tau}_1, f_1) &= F_{\Gamma_2}(\boldsymbol{\tau}_2, f_2) + (f_1 - f_2)|\Omega| - \int_{\Omega_{s,1}} \frac{(|\tau_1 - \tau_{s,Y}| + \tau_1 - \tau_{s,Y})^{1+1/n_s}}{(1+1/n_s)\kappa_s^{1/n_s} 2^{1+1/n_s}} \,\mathrm{d}\Omega \\
&\quad + \int_{\Omega_{s,2}} \frac{(|\tau_2 - \tau_{s,Y}| + \tau_2 - \tau_{s,Y})^{1+1/n_s}}{(1+1/n_s)\kappa_s^{1/n_s} 2^{1+1/n_s}} \,\mathrm{d}\Omega \\
&= F_{\Gamma_2}(\boldsymbol{\tau}_2, f_2) + \int_{\Omega_{s,2}|\Omega_{s,1}} \frac{(|\tau_2 - \tau_{s,Y}| + \tau_2 - \tau_{s,Y})^{1+1/n_s}}{(1+1/n_s)\kappa_s^{1/n_s} 2^{1+1/n_s}} \,\mathrm{d}\Omega \\
&\quad + \int_{\Omega_{s,1}} \frac{(|\tau_2 - \tau_{s,Y}| + \tau_2 - \tau_{s,Y})^{1+1/n_s} - (|\tau_1 - \tau_{s,Y}| + \tau_1 - \tau_{s,Y})^{1+1/n_s}}{(1+1/n_s)\kappa_s^{1/n_s} 2^{1+1/n_s}} \,\mathrm{d}\Omega \\
&\quad + \int_{\Omega_{s,1}} (\boldsymbol{\tau}_1 - \boldsymbol{\tau}_2)\cdot\nabla w_1 \,\mathrm{d}\Omega \\
&\geqslant F_{\Gamma_2}(\boldsymbol{\tau}_2, f_2) + \int_{\Omega_{s,1}} (\boldsymbol{\tau}_1 - \boldsymbol{\tau}_2)\cdot\nabla w_1 \,\mathrm{d}\Omega \\
&\quad + \int_{\Omega_{s,1}} \frac{(|\tau_2 - \tau_{s,Y}| + \tau_2 - \tau_{s,Y})^{1+1/n_s} - (|\tau_1 - \tau_{s,Y}| + \tau_1 - \tau_{s,Y})^{1+1/n_s}}{(1+1/n_s)\kappa_s^{1/n_s} 2^{1+1/n_s}} \,\mathrm{d}\Omega.
\end{aligned}$$

However, the integrand in the above integrals over $\Omega_{s,1}$ is positive, by exactly the same steps as in the proof of theorem 1; hence

$$F_{\Gamma_1}(\boldsymbol{\tau}_1, f_1) \geqslant F_{\Gamma_2}(\boldsymbol{\tau}_2, f_2).$$

□

The consequence of Theorem 2 is as follows. We take any nested sequence of spacer domains $\{\Omega_{s,j}\}_{j=1}^{\infty}$ with $\Omega_{s,j+1} \subseteq \Omega_{s,j}$, $\Omega_{s,1} = \Omega$ and each corresponding Γ_j admissible. Let $(\boldsymbol{\tau}_j, f_j) \in S_{\Gamma_j}$ and w_j denote the constrained solutions, which are known to exist on each $\Omega_{s,j}$. We define the sequence of functionals, $F_{\Gamma_j}(\boldsymbol{\tau}_j, f_j)$ for each $\Omega_{s,j}$. Theorem 2 states that the sequence $\{F_{\Gamma_j}(\boldsymbol{\tau}_j, f_j)\}_{j=1}^{\infty}$ is increasing for as long as w_j is a static mud wall layer solution, i.e. for as long as the mud does not move. Potentially therefore, we can maximize $F_{\Gamma_j}(\boldsymbol{\tau}_j, f_j)$ over all admissible interfaces for which a constrained static mud wall layer solution exists and it is this maximization which will define the maximal static mud wall layer in generality.

3.1. *Eventual yielding of the mud*

For an increasing sequence of $F_\Gamma(\boldsymbol{\tau}, f)$, each corresponding to a constrained static mud wall layer solution on a nested domain, we are led to question whether eventually the mud layer must yield for suitably small Ω_s. Without such a situation occurring we are unlikely to be able to define a maximal static mud layer via any optimization problem.

A mathematical justification for this to occur is as follows. For simplicity, we assume that $n_s = n_m = 1$, although the general case can be treated by similar methods. First note that each general solution satisfies

$$a(w, w) + j(w) - L(f, w) = 0, \tag{3.6}$$

and if the solution is a constrained static mud layer solution then

$$\kappa_s a_s(w, w) + \tau_{s,Y} j_s(w) = (f - b)|\Omega|. \tag{3.7}$$

https://doi.org/10.1017/S0022112003004105 Published online by Cambridge University Press

Since $w \neq 0$, this shows that $f > b$. Furthermore, we have

$$\kappa_s a_s(w, w) \geqslant \kappa_s \lambda_{\Omega_s,0} \|w\|^2_{L^2(\Omega_s)} = \kappa_s \lambda_{\Omega_s,0} \|w\|^2_{L^2(\Omega)} \geqslant \kappa_s \lambda_{\Omega_s,0} \frac{\|w\|^2_{L^1(\Omega)}}{|\Omega|} \geqslant \kappa_s \lambda_{\Omega_s,0} |\Omega|, \tag{3.8}$$

where $\lambda_{\Omega_s,0}$ is the smallest positive eigenvalue of the negative Laplacian operator, on Ω_s, with homogeneous Dirichlet boundary conditions.

For most simple shaped domains it is commonly found that $\lambda_{\Omega_s,0} \sim d^2_{\Omega_s}$, in the limit $|\Omega_s| \to 0$, where d_{Ω_s} represents a linear dimension of Ω_s. Assuming this, we have $f - b \geqslant \kappa_s \lambda_{\Omega_s,0} \sim \kappa_s [d_{\Omega_s}]^{-2}$ as $|\Omega_s| \to 0$. Thus, we have $\tau \sim (f - b) d_{\Omega_s} \sim \kappa_s [d_{\Omega_s}]^{-1} \to \infty$ as $|\Omega_s| \to 0$, and eventually the mud yield stress is exceeded. Physically, as explained in § 1, we are trying to force a fixed flow rate of spacer through a progressively smaller area. Eventually the pressure gradient required exerts so much stress on the mud layer that it yields.

3.2. *Numerical implementation and strategies for finding the maximal layer*

A general method for finding the maximal layer would consist of finding the constrained solution for a given interface position and then varying the interface position to maximize $F_\Gamma(\boldsymbol{\tau}, f)$. We note that in order for the static flow constraint to be satisfied it is both necessary and sufficient that $\tau \leqslant \tau_{k,Y}$ for $(x, y) \in \Omega_m$. Two general methodologies appear feasible:

(*a*) For given interface we find directly the constrained solution on Ω. We check that either the velocity is zero in Ω_m or (equivalently) that the stress does not exceed the yield stress in Ω_m. (Depending on the application one of these methods may be more convenient than the other.)

(*b*) We can assume *a priori* that the static flow constraint is satisfied. In this case we solve the constrained problem only on Ω_s, i.e. we impose homogeneous Dirichlet conditions on the boundary of Ω_s. Having solved the constrained problem on Ω_s we try to reconstruct the stress outside Ω_s and verify whether or not the yield stress is exceeded. Only if the yield stress is not exceeded will our *a priori* assumption be correct.

We note that these two methodologies are feasible only because if (w, f) is a constrained static mud wall layer solution, it is also a constrained solution for the homogeneous Dirichlet problem on Ω_s. If the geometry is relatively simple (e.g. a one-dimensional problem), we are often able to solve the single fluid problem more-or-less analytically, and thus the second methodology is preferred. For more complex geometries it will generally be easier to use the first method.

We note that Theorem 2 only states that $F_\Gamma(\boldsymbol{\tau}, f)$ increases in the direction of the maximal static wall layer. There is no reason for $F_\Gamma(\boldsymbol{\tau}, f)$ to start to decrease once the mud layer yields, i.e. identification of yielding requires that the stress field be examined. Therefore, for a general numerical implementation it will be advisable to add a penalty function term to the functional $F_\Gamma(\boldsymbol{\tau}, f)$, chosen in such a way that a maximum is achieved close to the maximal static wall layer. Thus, we should consider minimization of a functional $M_\Gamma(\boldsymbol{\tau}, f)$ of general form

$$M_\Gamma(\boldsymbol{\tau}, f) = -F_\Gamma(\boldsymbol{\tau}, f) + P_\Gamma(u). \tag{3.9}$$

The penalty function $P_\Gamma(u)$ needs to be chosen to be zero when the mud has not yielded and to increase sharply as soon as the mud layer yields. For the examples we consider later only simple solutions are studied and the penalty function is not

https://doi.org/10.1017/S0022112003004105 Published online by Cambridge University Press

strictly necessary. For more complex geometries a second penalty function might also be added to ensure some regularity of the interface.

Secondly, for efficient computational implementation, it is necessary to compute the shape derivatives of $M_\Gamma(\boldsymbol{\tau}, f)$. This is not straightforward for the flows we consider, and is the subject of ongoing research. We comment that, for the case where the spacer is Newtonian, this amounts to computing the shape derivatives of the solution of Poisson's equation on a Lipschitz continuous domain. Results relevant to this problem and to shape optimization of a number of problems governed by elliptic variational inequalities are given in Sokolowski & Zolesio (1991).

3.3. *Parametric dependence of the maximal static mud wall layer*

Suppose we adopt strategy (b) above and solve the constrained Dirichlet problem on Ω_s. It is apparent that there is one dimensionless parameter too many in the problem specification. For example, dividing (2.2) by $\tau_{s,Y}$, we see that the solution $(w, f/\tau_{s,Y})$ is a function only of n_s, $b/\tau_{s,Y}$ and the ratio, $\tau_{s,Y}/\kappa_s$. The solution thus computed results in a stress field within Ω_m, which is scaled by $\tau_{s,Y}$, and for which the only question that we examine is whether or not the magnitude of the stress field exceeds $\tau_{m,Y}/\tau_{s,Y}$ in Ω_m. Therefore, our computation of the maximal residual wall layer yields a solution that depends on the following parameters only:

$$n_s, \quad \varphi_B = \frac{b}{\tau_{m,Y}}, \quad B_s = \left(\frac{\tau_{s,Y}}{\kappa_s}\right)^{1/n_s}, \quad \varphi_Y = \frac{\tau_{s,Y}}{\tau_{m,Y}}. \tag{3.10}$$

Note that we have re-scaled b with $\tau_{m,Y}$ above to allow the possibility of $\tau_{s,Y} = 0$, and have introduced the spacer Bingham number, B_s, instead of only the ratio $\tau_{s,Y}/\kappa_s$; see e.g. §4.1 for how B_s occurs naturally in these flows. Furthermore, in solving the constrained Dirichlet problem on Ω_s, the pressure gradient term is $f - b$, not f. Thus in fact, it is the solution $(w, (f-b)/\tau_{s,Y})$, which is a function only of n_s and B_s. In the critical case, where the maximal static mud layer is $\Omega_s = \emptyset$, the effects of buoyancy are therefore not felt, i.e. we consider only the wall shear stress when $\Omega = \Omega_s$. Hence, the criterion of having no maximal layer possible depends solely on n_s, B_s and φ_Y.

4. Numerical examples

4.1. *Maximal mud layers in a slot*

The geometrically simplest example, with which to illustrate the key features of a maximal static wall layer and to demonstrate the feasibility of using a minimization such as (3.9), is the flow of two Herschel–Bulkley fluids in a plane channel (slot), which is symmetric about the centreline. The case for two Bingham fluids has been considered in Allouche *et al.* (2000), in a slightly different context. Here we adopt the direct approach (b) outlined in §3 above, solving the constrained Dirichlet problem on Ω_s and afterwards verifying that the mud has not yielded.

4.1.1. *Computing the maximal layer h_{max} directly*

Suppose then that $\Omega = (0, 1)$, $\Omega_s = (0, y_i)$ and $\Omega_m = (y_i, 1)$, that $(b, \tau_{k,Y}, \kappa_k, n_k)$: $k = m, s$ are fixed; we shall find the minimal y_i, say $y_{i,min}$, for which the mud layer remains static.† Boundary conditions for the full problem are no slip at $y = 1$ and

† Note that for the slot we actually have $\Omega = \Omega \times [-\infty, \infty]$. Implicit here is the assumption of uniformity in the (suppressed) x-direction, which allows us to apply the results of the previous sections. See also §4.1.3.

https://doi.org/10.1017/S0022112003004105 Published online by Cambridge University Press

zero shear stress at $y = 0$. The momentum equations can be integrated to give

$$\tau_{s,zy} = -(f-b)y, \qquad y \in [0, y_i], \tag{4.1}$$

$$\tau_{m,zy} = by_i - fy, \qquad y \in (y_i, 1], \tag{4.2}$$

where $f - b > 0$ to ensure a positive flow rate and we seek the minimal $y_{i,min}$ for which $|\tau_{m,zy}(y=1)| \leqslant \tau_{m,Y}$, which would imply that $w(y) = 0 : \quad y \in (y_i, 1)$.

For this we must solve the constrained Dirichlet problem on $(0, y_i)$, using (4.1), $w(y_i) = 0$, and the following simplified constitutive laws:

$$|w'(y)| = 0 \Longleftrightarrow |\tau_{s,zy}| \leqslant \tau_{s,Y}, \tag{4.3}$$

$$\tau_{s,zy} = \left[\kappa_s |w'(y)|^{n_s - 1} + \frac{\tau_{s,Y}}{|w'(y)|}\right] w'(y) \Longleftrightarrow |\tau_{s,zy}| > \tau_{s,Y}. \tag{4.4}$$

We define y_Y, the yield surface, by

$$y_Y = \tau_{s,Y}/(f-b), \tag{4.5}$$

and integrate to find

$$w(y) = \begin{cases} B_s \dfrac{[y_i - y_Y]^{m_s+1}}{(m_s+1)y_Y^{m_s}}, & y \in [0, y_Y], \\ B_s \dfrac{[y_i - y_Y]^{m_s+1} - [y - y_Y]^{m_s+1}}{(m_s+1)y_Y^{m_s}}, & y \in (y_Y, y_i], \end{cases} \tag{4.6}$$

where $m_s = 1/n_s$ and B_s is defined in (3.10). Integrating between $y = 0$ and $y = y_i$ we find

$$\int_0^{y_i} w(y)\,\mathrm{d}y = B_s y_i^2 \frac{[y_i/y_Y - 1]^{m_s}[1 - y_Y/y_i][m_s + 1 + y_Y/y_i]}{(m_s+1)(m_s+2)}$$

$$= B_s y_i^2 \frac{[1/y^* - 1]^{m_s}[1 - y^*][m_s + 1 + y^*]}{(m_s+1)(m_s+2)},$$

where $y^* = y_Y/y_i < 1$. Thus, in order to find the solution of the constrained problem with flow constraint

$$\int_0^{y_i} w(y)\,\mathrm{d}y = Q_s \tag{4.7}$$

we find the zero $y^* \in (0, 1)$, of the nonlinear equation

$$G_{m,B,Q}(y^*) = 0 : \quad G_{m,B,Q}(y^*) \equiv B[1 - y^*]^{m+1}[1 + m + y^*] - (m+1)(m+2)Q(y^*)^m, \tag{4.8}$$

for positive parameters

$$m = m_s, \quad B = y_i^2 B_s, \quad Q = Q_s.$$

The existence of a unique solution to this equation follows from § 2.4. Thus fixing $Q_s = 1$, we find that $y_Y = y_Y(m_s, B_s, y_i)$ and hence

$$|\tau_{m,zy}(y=1)| = f - by_i = f - b + (1 - y_i)b = \frac{\tau_{s,Y}}{y_Y(m_s, B_s, y_i)} + (1 - y_i)b,$$

and to find the minimal value of y_i we solve

$$\frac{\tau_{s,Y}}{y_Y(m_s, B_s, y_{i,min})} + (1 - y_{i,min})b = \tau_{m,Y} \Longleftrightarrow \frac{\varphi_Y}{y_Y(1/n_s, B_s, y_{i,min})} + (1 - y_{i,min})\varphi_B = 1, \tag{4.9}$$

https://doi.org/10.1017/S0022112003004105 Published online by Cambridge University Press

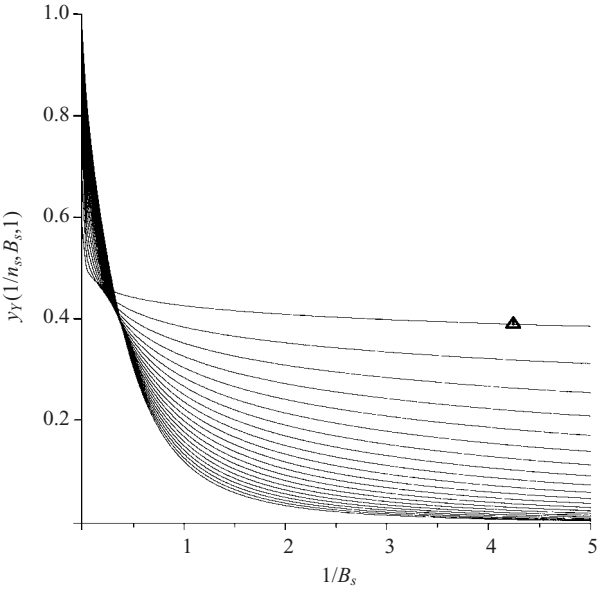


FIGURE 2. The limiting yield stress ratio φ_Y required so that there can be a static wall layer: $\varphi_Y = y_Y(1/n_s, B_s, 1)$. Curves of $y_Y(1/n_s, B_s, 1)$ plotted against $1/B_s$, for $n_s = 0.1,\ 0.2,\ 0.3, \ldots, 2.0$. The curve $n_s = 0.1$ is marked with a triangle.

with φ_Y and φ_B defined in (3.10). The critical condition where there is no mud at all, $y_{i,min} = 1$, is therefore given by $\varphi_Y = y_Y(1/n_s, B_s, 1)$, which is independent of the buoyancy terms (φ_B). This has the curious physical interpretation that there will be no mud left on the wall if the fraction of the width of unyielded spacer, which would flow down the channel in a single fluid flow, exceeds the ratio of yield stresses in the two fluids. In figure 2 we show this limiting yield stress ratio $\varphi_Y = y_Y(1/n_s, B_s, 1)$, for increasing values of n_s. For small B_s, shear-thinning fluids ($n_s < 1$) require a higher yield stress than shear-thickening fluids ($n_s > 1$), in order to remove mud from the wall. For large B_s this trend is reversed.

We define the maximal static layer thickness h_{max} by

$$h_{max} = h_{max}(n_s, B_s, \varphi_Y, \varphi_B) = 1 - y_{i,min}(n_s, B_s, \varphi_Y, \varphi_B). \tag{4.10}$$

In figure 3 we show the variation in $h_{max}(n_s, B_s, \varphi_Y, \varphi_B)$ with each of its independent parameters: h_{max} decreases with n_s; h_{max} increases with B_s; h_{max} decreases with φ_Y; h_{max} decreases with φ_B.

4.1.2. *The functional* $F_\Gamma(\boldsymbol{\tau}, f)$

To evaluate $F_\Gamma(\boldsymbol{\tau}, f)$ for our simple example, we substitute from § 4.1.1 into (3.4), noting that $|\Omega| = 1$. After some algebra we derive

$$F_\Gamma(\boldsymbol{\tau}, f) = (f - b)\left\{1 - \frac{B_s y_i^2 (1 - y^*)^{m_s+2}}{(m_s + 1)(m_s + 2)(y^*)^{m_s}}\right\}, \tag{4.11}$$

and we note from (4.8) that

$$1 = \frac{B_s y_i^2 (1 - y^*)^{m_s+1}(m_s + 1 + y^*)}{(m_s + 1)(m_s + 2)(y^*)^{m_s}},$$

https://doi.org/10.1017/S0022112003004105 Published online by Cambridge University Press

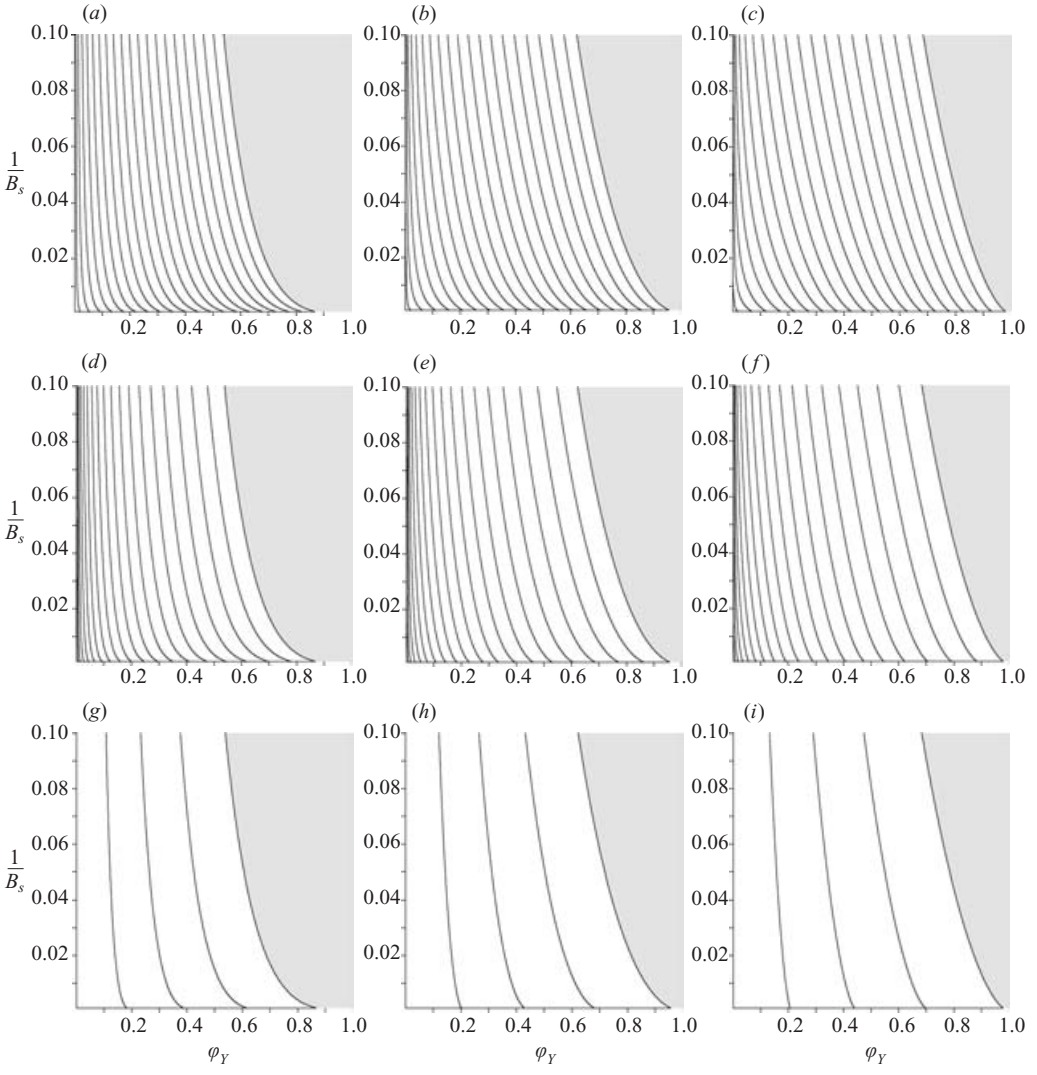


FIGURE 3. Maximal static wall layer $h_{max} = h_{max}(n_s, B_s, \varphi_Y, \varphi_B)$ for $\varphi_Y \in [0.001, 1]$, $1/B_s \in [0.001, 0.1]$; contours spaced at intervals $\Delta h_{max} = 0.05$: (*a*) $\varphi_B = 0$, $n_s = 0.5$; (*b*) $\varphi_B = 0$, $n_s = 1.0$; (*c*) $\varphi_B = 0$, $n_s = 1.5$; (*d*) $\varphi_B = 1.0$, $n_s = 0.5$; (*e*) $\varphi_B = 1.0$, $n_s = 1.0$; (*f*) $\varphi_B = 1.0$, $n_s = 1.5$; (*g*) $\varphi_B = 5.0$, $n_s = 0.5$; (*h*) $\varphi_B = 5.0$, $n_s = 1.0$; (*i*) $\varphi_B = 5.0$, $n_s = 1.5$.

for a constrained static wall layer solution, $Q_s = 1$. Thus, finally

$$F_\Gamma(\boldsymbol{\tau}, f) = (f - b)\frac{m_s + 2y^*}{1 + m_s + y^*}. \tag{4.12}$$

Some computed examples are shown in figure 4, for both shear-thinning and shear-thickening fluids. Two points are evident from figure 4. First, F_Γ is indeed increasing for increasing h (i.e. nested Ω_s), as is stated in Theorem 2. Second, we have marked in figure 4 the computed value of h_{max} for each set of parameters. The function F_Γ has been continued through $h = h_{max}$ and continues to increase. Thus, in using any optimization approach to find the maximal static wall layer, it is clear that the

https://doi.org/10.1017/S0022112003004105 Published online by Cambridge University Press

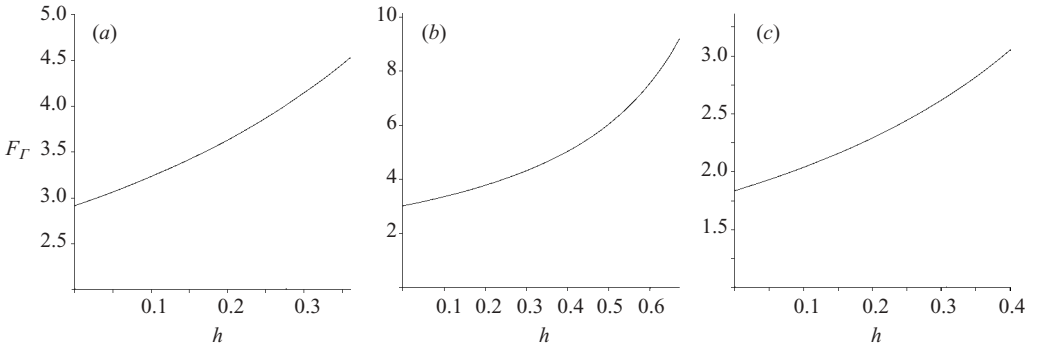


FIGURE 4. The functional $F_\Gamma(\boldsymbol{\tau}, f) = F_\Gamma(h)$, defined by (3.4), plotted for varying mud layer thicknesses h: (*a*) $n_s = 1$, $\tau_{s,Y} = 1$, $\kappa_s = 1$, $\tau_{m,Y} = 10$, $b = 0$; (*b*) $n_s = 0.5$, $\tau_{s,Y} = 2$, $\kappa_s = 0.5$, $\tau_{m,Y} = 10$, $b = 2$; (*c*) $n_s = 1.5$, $\tau_{s,Y} = 1$, $\kappa_s = 0.25$, $\tau_{m,Y} = 8$, $b = 3$. In each case the vertical dashed line marks the position of h_{max}.

minimizer will lie on the boundary of the set of feasible Γ. In using an approach such as (3.9), we will therefore require a penalty function and/or some sort of indicator function in order to signal that the boundary of the set of feasible Γ has been attained.

4.1.3. *Instability and the tendency to bridge the gap*

As mentioned, in reality the plane channel of §4.1.1 has a third spatial direction: x. It is natural to ask whether the solution computed in §4.1.1 would be maximal in a three-dimensional plane channel, i.e. in three dimensions does the maximal static layer solution correspond to that with h_{max} uniform in x? It might be for example, that a thicker total mud layer is achieved by a non-uniform static mud layer that shows a tendency to bridge the gap between the parallel plates at certain points whilst compensating with a thinner layer elsewhere.

To see whether this tendency exists, it suffices to consider identical two plane channels, connected in parallel. A fixed flow rate $Q = 1$ is imposed, but we allow Q_1 to pass through channel 1 and Q_2 through channel 2, where $Q_1 + Q_2 = 1$. For $Q_1 \in [0, 1]$ we compute $h_{max}(Q_1)$ for channel 1 and $h_{max}(1 - Q_1)$ for channel 2, using an obvious adaptation of the methods in §4.1.1, for $Q \neq 1$. In figure 5 we plot $h_{max}(Q_1)$, $h_{max}(1 - Q_1)$ and $h_{max}(Q_1) + h_{max}(1 - Q_1)$. We have fixed $n_s = 1 = B_s$, $\varphi_Y = 0.1$, $\varphi_B = 0$, but qualitatively similar results are found for all parameters that we have explored.

It is evident from figure 5 that the total maximal static wall layer will be found when either $Q_1 = 0$ or $Q_2 = 0$, i.e. one of the channels is completely blocked. Considering a single plane channel with a sufficiently long aspect in the x-direction, it is evident that a tendency to bridge the channel in certain places will bring about a static layer which is thicker overall than the uniform solution of §4.1.1. Presumably, in non-uniform duct geometries, such as the eccentric annulus, the duct geometry acts to select where the mud layer will bridge.

4.2. *Mud layers forming in a concentric annulus*

The second geometrically simple example that we consider is a uniform concentric annulus, for which an axisymmetric solution is possible. For simplicity, we consider only the case $n_s = n_m = 1$. We denote the annulus by $r \in [r_i, 1]$ and the spacer region by $\Omega_s : r \in (r_1, r_2)$. Three different problems are considered: two single mud layer

https://doi.org/10.1017/S0022112003004105 Published online by Cambridge University Press

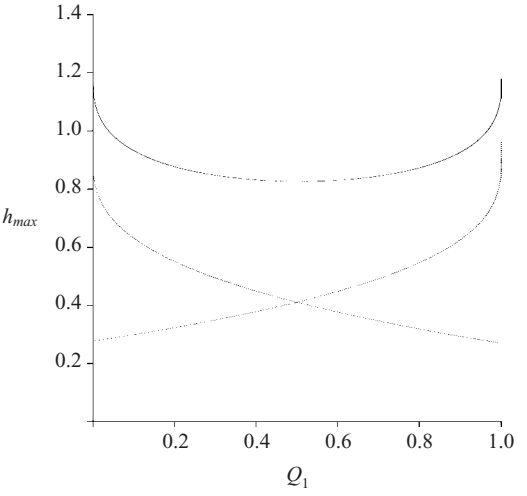


FIGURE 5. Plots of $h_{max}(Q_1)$, $h_{max}(1-Q_1)$ (lower lines) and $h_{max}(Q_1)+h_{max}(1-Q_1)$ (upper line) for $n_s = 1 = B_s$, $\varphi_Y = 0.1$, $\varphi_B = 0.0$.

problems, for which the mud layer is either on the inside or outside wall (i.e. either $r_1 = r_i$ or $r_2 = 1$), and also briefly the double mud layer problem. The momentum equations are simply

$$\frac{1}{r}\frac{\mathrm{d}}{\mathrm{d}r}(r\tau_s) = -(f-b), \qquad r \in \Omega_s, \tag{4.13}$$

$$\frac{1}{r}\frac{\mathrm{d}}{\mathrm{d}r}(r\tau_m) = -f, \qquad r \in \Omega_m, \tag{4.14}$$

with constitutive relations

$$|w'(r)| = 0 \Longleftrightarrow |\tau_s| \leqslant \tau_{s,Y}, \tag{4.15}$$

$$|w'(r)| > 0 \Longleftrightarrow |\tau_s| > \tau_{s,Y} \Longrightarrow \tau_s(r) = \left(\kappa_s + \frac{\tau_{s,Y}}{|w'(r)|}\right) w'(r). \tag{4.16}$$

As for the slot, we work primarily with the Dirichlet problem for the spacer, i.e. assuming that the mud layer is static and then determining the stresses exerted on it, for verification. For a static mud layer, no-slip boundary conditions are applied at $r = r_i$ and $r = 1$. The stress in the spacer is given by

$$\tau_s(r) = -\frac{f-b}{2}\left(r - \frac{{r_0}^2}{r}\right), \tag{4.17}$$

where $\tau_s(r_0) = 0$. Note that $f - b > 0$ to ensure a positive flow rate. Since $w'(r)$ has the same sign as $\tau_s(r)$, in order to satisfy the no-slip conditions at $r = r_1$ and $r = r_2$ it is clear that we will need $r_0 \in (r_1, r_2)$. Thus, we expect that the solution will have a single unyielded plug region for $r \in (r_1, r_2)$. We denote the boundaries of the plug region $r = r_{Y\pm}$, where we have

$$\pm\tau_{s,Y} = -\frac{f-b}{2}\left(r_{Y\pm} - \frac{{r_0}^2}{r_{Y\pm}}\right). \tag{4.18}$$

https://doi.org/10.1017/S0022112003004105 Published online by Cambridge University Press

Denoting $r_Y = \tau_{s,Y}/(f-b)$ we find that the two yield surfaces are at

$$r_{Y^+} = -r_Y + \sqrt{r_Y^2 + r_0^2}, \tag{4.19}$$

$$r_{Y^-} = r_Y + \sqrt{r_Y^2 + r_0^2}. \tag{4.20}$$

Thus, $\tau_s(r) = \pm\tau_{s,Y}$ at $r = r_{Y^\pm}$, with r_{Y^+} denoting the inner yield surface and r_{Y^-} denoting the outer yield surface. Expressions for the velocity may now be constructed in both yielded layers $r \in (r_1, r_{Y^+})$ and $r \in (r_{Y^-}, r_2)$, by using the constitutive laws and integrating inwards from the static mud–spacer interfaces at $r = r_1$ and r_2. These expressions depend only on the two unknowns r_0 and r_Y, and are parameterized by the spacer Bingham number B_s, see (3.10).

We determine r_0 and r_Y by the following two conditions: (i) the velocity must be continuous across the plug region; (ii) the mean velocity averaged over the annulus is equal to 1. The velocities at the unyielded plug, determined by integrating away from the static mud–cement interface in each yielded layer, are denoted $w_{Y^\pm}$ at $r = r_{Y^\pm}$:

$$w_{Y^+} = B_s\left(\frac{1}{2r_Y}\left(\frac{r_1^2 - r_{Y^+}^2}{2}\right) + \frac{r_0^2}{2r_Y}\ln\left(\frac{r_{Y^+}}{r_1}\right) + r_1 - r_{Y^+}\right), \tag{4.21}$$

$$w_{Y^-} = B_s\left(\frac{1}{2r_Y}\left(\frac{r_2^2 - r_{Y^-}^2}{2}\right) - \frac{r_0^2}{2r_Y}\ln\left(\frac{r_2}{r_{Y^-}}\right) - r_2 + r_{Y^-}\right). \tag{4.22}$$

From (4.19) and (4.20), we see that $|r_{Y^+} - r_1|$ increases with r_0 and $|r_2 - r_{Y^-}|$ decreases with r_0. Thus, it follows that $(w_{Y^+} - w_{Y^-})$ increases with r_0. Hence, for fixed $r_Y = \frac{1}{2}(r_{Y^-} - r_{Y^+}) \leqslant \frac{1}{2}(r_2 - r_1)$, we can solve

$$G_1(r_0, r_Y) = 0: \quad G_1(r_0, r_Y) \equiv w_{Y^+} - w_{Y^-} \tag{4.23}$$

to give r_0, and hence have found $w(r)$ on $[r_1, r_2]$ satisfying $w(r_1) = w(r_2) = 0$ and continuity across the unyielded plug. Secondly, we need to satisfy the flow rate constraint given by

$$\tfrac{1}{2}\left(1 - r_i^2\right) = \int_{r_1}^{r_2} r\, w(r)\, \mathrm{d}r, \tag{4.24}$$

which becomes the following nonlinear equation, $G_2(r_0, r_Y) = 0$:

$$G_2(r_0, r_Y) \equiv \frac{B_s}{2r_Y}\left(\frac{r_{Y^+}^4 - r_1^4 + r_2^4 - r_{Y^-}^4}{4} + r_0\frac{r_1^2 - r_{Y^+}^2 + r_{Y^-}^2 - r_2^2}{2}\right) + B_s\frac{r_{Y^+}^3 - r_1^3 + r_{Y^-}^3 - r_2^3}{3} - \left(1 - r_i^2\right), \tag{4.25}$$

where implicitly $r_0 = r_0(r_Y) = r_0(f)$ has been found from (4.23). We take $r_Y = \frac{1}{2}(r_2 - r_1)$ as an upper limit for r_Y, we note that $f - b$ increases when r_Y decreases, and (see § 2.4) we know that the flow rate increases monotonically with the pressure gradient $f - b$. Hence, (4.25) also admits a unique solution. Rather than solve (4.23) and (4.25) sequentially as described, we compute (r_0, r_Y) together using a fixed point iteration for the system of nonlinear equations, $G_1(r_0, r_Y) = 0$ and $G_2(r_0, r_Y) = 0$. An example of this solution, showing both $w(r)$ and $\tau_s(r)$ is shown in figure 6.

Having found the solution to the constrained Dirichlet problem on (r_1, r_2), (which is parameterized only by B_s), the values of the stresses at the two interfaces are

https://doi.org/10.1017/S0022112003004105 Published online by Cambridge University Press

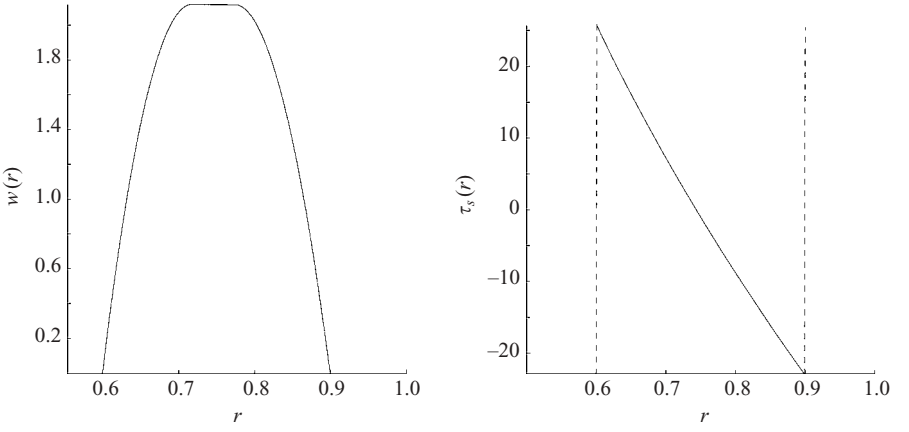


FIGURE 6. The velocity $w(r)$ and the stress profile $\tau_s(r)$ plotted for $r_i = 0.5$, $r_1 = 0.6$, $r_2 = 0.9$ and $B_s = 1.0$.

given by

$$\tau_{s,1} = \tau_s(r_1) = -\frac{f-b}{2}\left(r_1 - \frac{{r_0}^2}{r_1}\right), \tag{4.26}$$

$$\tau_{s,2} = \tau_s(r_2) = -\frac{f-b}{2}\left(r_2 - \frac{{r_0}^2}{r_2}\right). \tag{4.27}$$

The absolute value of the stress increases across the two unyielded mud layers, giving the following values at the inner and outer walls:

$$\tau_m(r_i) = \frac{f-b}{2r_i}\left(r_0^2 - r_i^2\right) + \frac{b}{2r_i}\left(r_1^2 - r_i^2\right) = \frac{\tau_{s,Y}}{2r_i r_Y}\left(r_0^2 - r_i^2\right) + \frac{b}{2r_i}\left(r_1^2 - r_i^2\right), \tag{4.28}$$

$$\tau_m(1) = -\frac{f-b}{2}\left(1 - r_0^2\right) - \frac{b}{2}\left(1 - r_2^2\right) = -\frac{\tau_{s,Y}}{2r_Y}\left(1 - r_0^2\right) - \frac{b}{2}\left(1 - r_2^2\right). \tag{4.29}$$

4.2.1. *Single mud wall layer problems*

Consider the case when there is a single mud layer in the annulus, on the outer wall. We fix $r_1 = r_i$ and seek the minimal r_2 for which the mud layer remains static, say $r_2 = r_{2,min}$. This is found when $\tau_m(1) = -\tau_{m,Y}$, so that $r_{2,min}$ satisfies

$$\tau_{m,Y} = \frac{\tau_{s,Y}}{2r_Y}\left(1 - r_0^2\right) + \frac{b}{2}\left(1 - r_{2,min}^2\right) \Longleftrightarrow \frac{\varphi_Y}{r_Y}\left(1 - r_0^2\right) + \varphi_B\left(1 - r_{2,min}^2\right) = 2, \tag{4.30}$$

with φ_Y and φ_B defined in (3.10). Similarly, we can consider the case in which there is a single mud layer on the inner wall and $r_2 = 1$. The maximal r_1 for which the mud layer remains static, say $r_{1,max}$, is found when $\tau_m(r_i) = \tau_{m,Y}$. Hence, $r_{1,max}$ satisfies

$$\tau_{m,Y} = \frac{\tau_{s,Y}}{2r_i r_Y}\left(r_0^2 - r_i^2\right) + \frac{b}{2r_i}\left(r_{1,max}^2 - r_i^2\right) \Longleftrightarrow \frac{\varphi_Y}{r_i r_Y}\left(r_0^2 - r_i^2\right) + \varphi_B\left(r_{1,max}^2 - r_i^2\right) = 2. \tag{4.31}$$

We note that $r_{2,min}$ and $r_{1,max}$ depend parametrically on r_i, B_s, φ_Y and φ_B, as expected.

Actual values of $r_{2,min}$ and $r_{1,max}$ are computed straightforwardly from (4.30) and (4.31). In figures 7 and 8 respectively, we show results of this computation for $r_{2,min}$ and $r_{1,max}$. Identical parameters are used in figures 7 and 8, to enable comparison.

https://doi.org/10.1017/S0022112003004105 Published online by Cambridge University Press

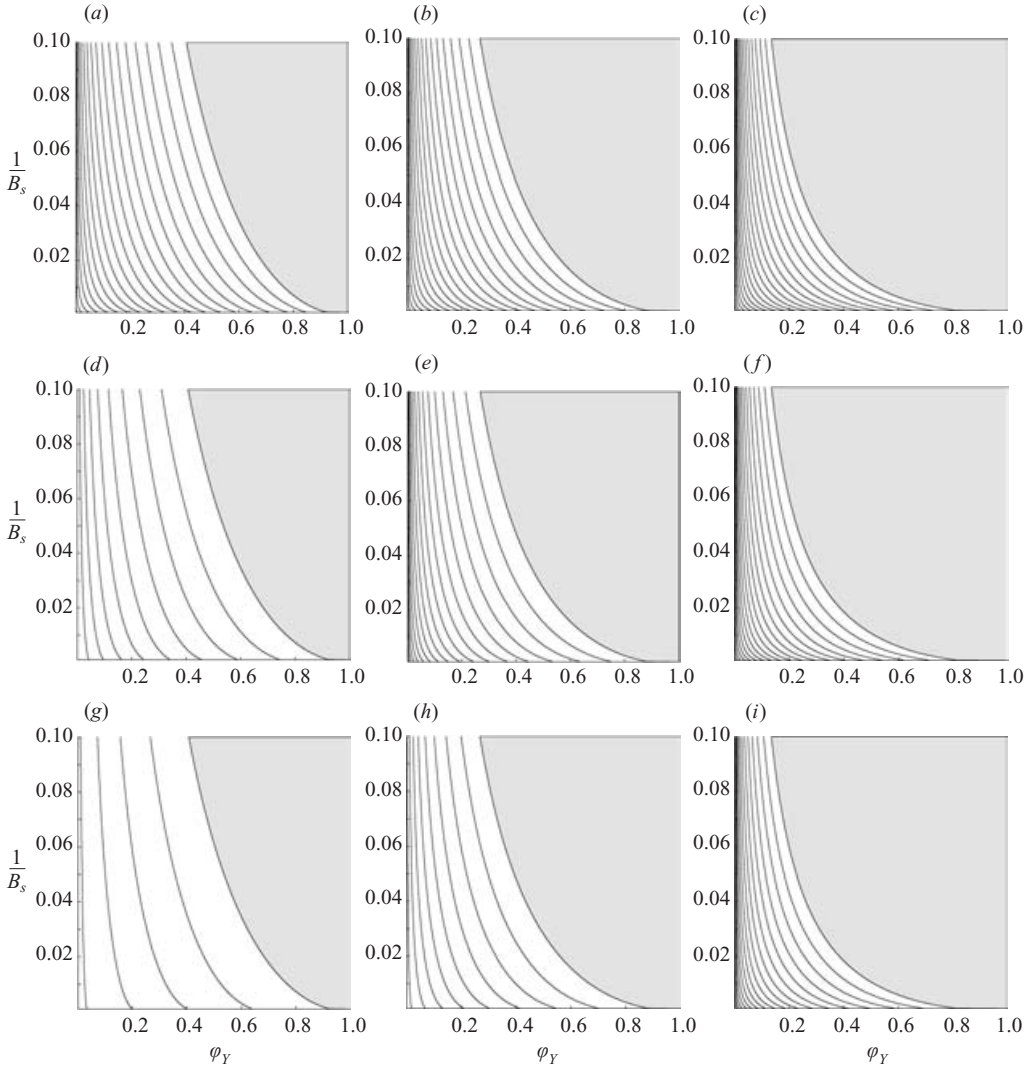


FIGURE 7. Maximal static wall layer h_{max} for a single layer on the outer wall: $\varphi_Y \in [0.001, 1]$, $1/B_s \in [0.001, 0.1]$; contour spacing 0.02. (*a*) $\varphi_B = 0.0$, $r_i = 0.5$; (*b*) $\varphi_B = 0.0$, $r_i = 0.75$; (*c*) $\varphi_B = 0.0$, $r_i = 0.9$; (*d*) $\varphi_B = 5.0$, $r_i = 0.5$; (*e*) $\varphi_B = 5.0$, $r_i = 0.75$; (*f*) $\varphi_B = 5.0$, $r_i = 0.9$; (*g*) $\varphi_B = 10.0$, $r_i = 0.5$; (*h*) $\varphi_B = 10.0$, $r_i = 0.75$; (*i*) $\varphi_B = 10.0$, $r_i = 0.9$. In the shaded areas there is no layer.

Rather than plot $r_{2,min}$ and $r_{1,max}$ directly, we have chosen to present contours of the normalized maximal layer thickness $h_{max}(r_i, B_s, \varphi_Y, \varphi_B)$:

$$h_{max} = \frac{1 - r_{2,min}}{1 - r_i} \quad \text{(outer layer)}, \qquad h_{max} = \frac{r_{1,max} - r_i}{1 - r_i} \quad \text{(inner layer)},$$

i.e. h_{max} represents the proportion of the annular gap occupied by the maximal mud layer.

In comparing the results in figures 7 and 8, it can be observed that for a narrow gap $r_i \sim 1$, the inner and outer layers results approach one another. This is to be expected since the effects of curvature are minimized. For smaller r_i there are discernible

https://doi.org/10.1017/S0022112003004105 Published online by Cambridge University Press

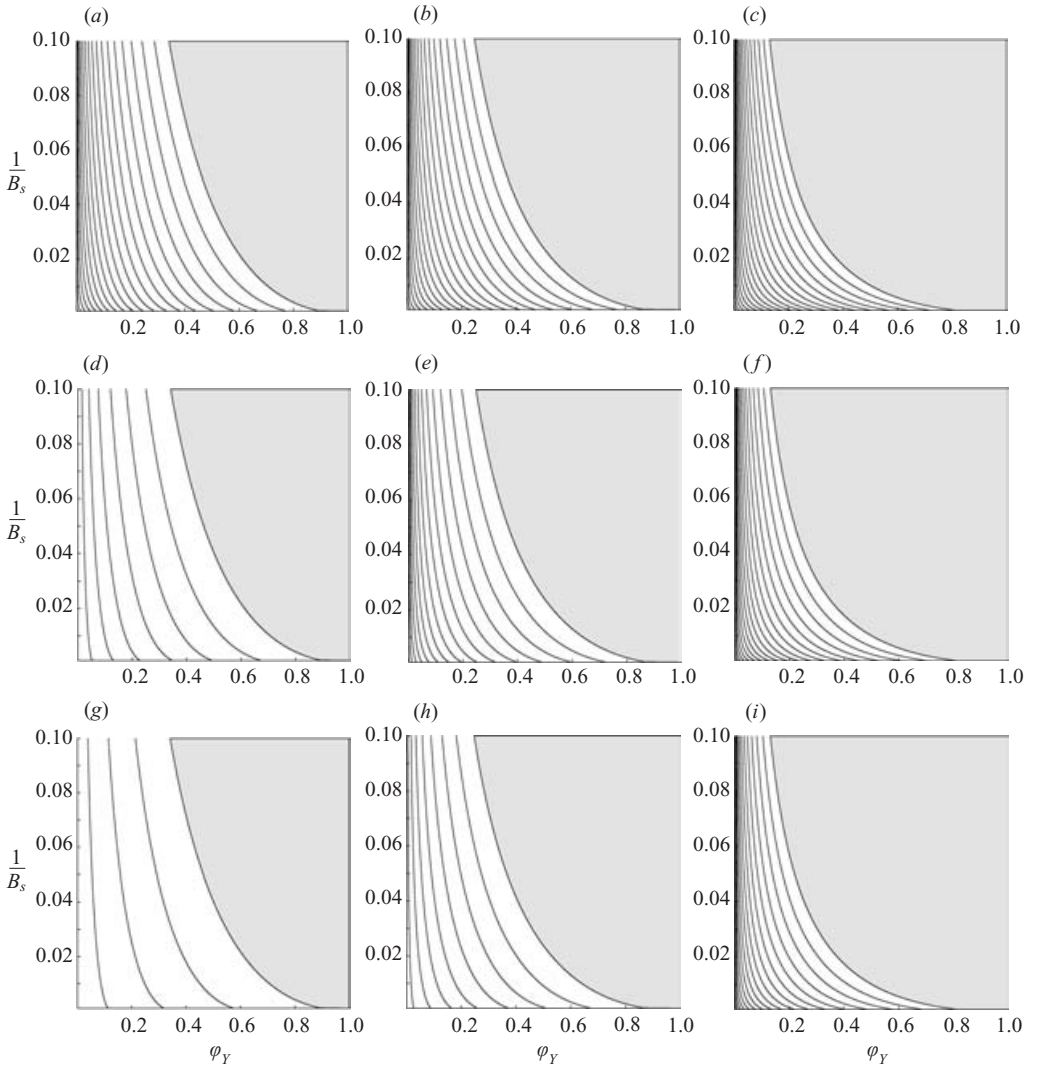


FIGURE 8. As figure 7 but for a single layer on the inner wall.

differences between inner and outer maximal layer thicknesses. In general the outer maximal layer is thicker than the inner maximal layer. Note that if $r_{2,min} = 1$ or if $r_{1,max} = r_i$, there is no mud layer at all. These limits can be computed directly and give the following relations:

$$\frac{\varphi_Y}{r_Y}\left(1 - r_0^2\right) \geqslant 2 \Longrightarrow \quad \text{no outer wall layer,} \tag{4.32}$$

$$\frac{\varphi_Y}{r_i r_Y}\left(r_0^2 - r_i^2\right) \geqslant 2 \Longrightarrow \quad \text{no inner wall layer.} \tag{4.33}$$

The difference in layer thickness is most visible by plotting the shaded areas where there is no layer, for both inner and outer layer problems of figures 7 and 8, as shown in figure 9.

https://doi.org/10.1017/S0022112003004105 Published online by Cambridge University Press

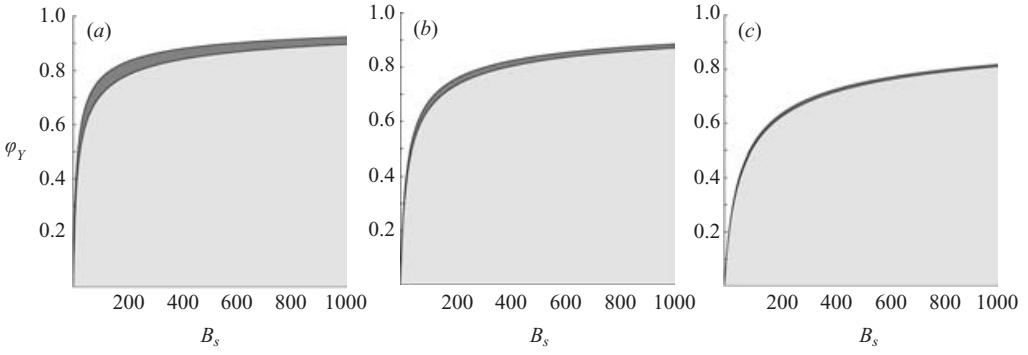


FIGURE 9. The regions in which there exist no static layers for inner (shaded dark) and outer (shaded light) layer problems: $r_i = 0.5$: (*a*) $\varphi_B = 0.0$, $r_i = 0.5$; (*b*) $\varphi_B = 5.0$, $r_i = 0.5$; (*c*) $\varphi_B = 10.0$, $r_i = 0.5$.

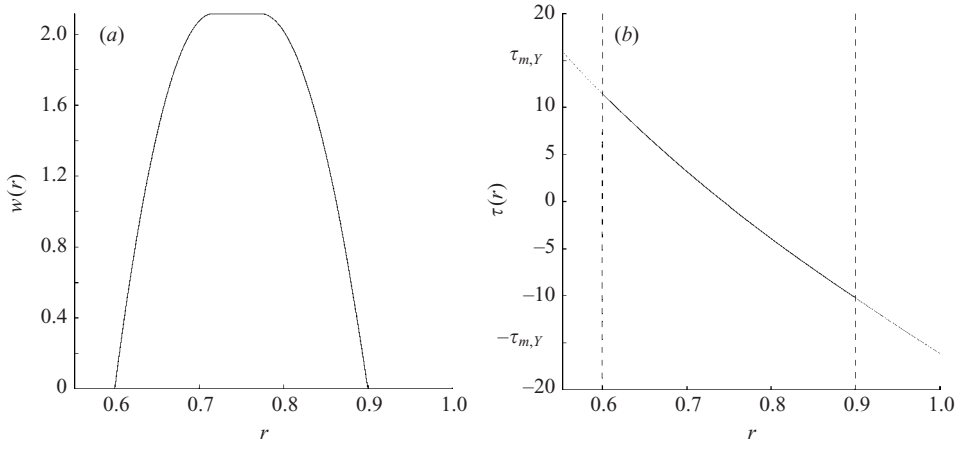


FIGURE 10. The velocity $w(r)$ and the stress profiles $\tau_s(r)$ and $\tau_m(r)$ plotted for $\tau_{s,Y} = 2$, $\kappa_s = 0.25$, $b = 1$ and $(r_{1,max}, r_{2,min}) = (0.6, 0.9)$.

4.2.2. *Double layer problem*

Finally we consider briefly the double layer problem. The aim here is simply to illustrate that the functional $F_\Gamma(\boldsymbol{\tau}, f)$ is increasing with nested Ω_s and can, when augmented with a suitable penalty function, be used in a minimization problem for the maximal layer. The solution of this problem is mainly of interest as a test problem for a fully two-dimensional shape optimization. Having found a constrained solution, evaluation of $F_\Gamma(\boldsymbol{\tau}, f)$ is a straightforward but algebraically tedious task. We do not present the long expression for $F_\Gamma(\boldsymbol{\tau}, f)$ here.

In figure 10 we illustrate a maximal mud layer solution for the double layered problem, showing both $w(r)$ and $\tau_k(r)$: $k = s, m$. By choice of a suitable penalty function, see figure 11, it is obviously possible to find the same maximal layers by the solution of a minimization problem with the objective functional of form (3.9). There are many choices of penalty function possible, and we have simply taken a penalty functional $P_\Gamma(\boldsymbol{\tau}, f)$:

$$P_\Gamma(\boldsymbol{\tau}, f) = C(H(\tau_m(r_i) - \tau_{m,Y})[\tau_m(r_i) - \tau_{m,Y}]^2 + H(-\tau_m(1) - \tau_{m,Y})[\tau_m(1) + \tau_{m,Y}]^2),$$

https://doi.org/10.1017/S0022112003004105 Published online by Cambridge University Press

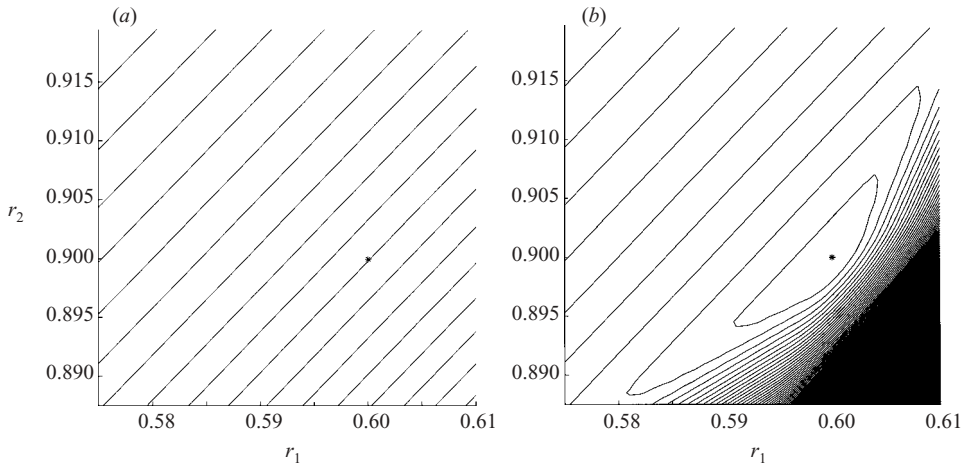


FIGURE 11. Contour plots of the functionals (*a*) $-F_\Gamma(\boldsymbol{\tau}, f)$, (*b*) $-F_\Gamma(\boldsymbol{\tau}, f) + P_\Gamma(\boldsymbol{\tau}, f)$, with (r_1, r_2), for the same parameters as in figure 10. The maximal mud layer is marked with a star.

where $H(x)$ is the Heaviside function and $C > 0$ is an appropriately chosen constant.

5. Discussion

For any process in which residual layers of material are left on the walls of a duct, the notion of a maximal layer is physically natural. The main thrust of the paper has been towards defining this notion more rigorously and in a way which allows general computation. To this end, derivation of the functional F_Γ and demonstration that F_Γ increases with nested interfaces for any series of static wall layer solutions (see Theorem 2) is perhaps the most useful general contribution made.

It is evident that this type of result can be generalized to other cleaning situations that involve steady flows governed by the Stokes equations. Our choice of axial duct flows is perhaps the easiest, but also one with many practical applications. The characterization of the residual fluid as a Herschel–Bulkley fluid is only relevant insofar as it has a yield stress (although the more general results of §2 clearly rely on the yielded behaviour). In considering those processes in which the residual fluid might be modelled as having a yield stress, the model is most appropriate for considering gelled or unyielded non-Newtonian fluids, or newly formed soft solids. For example, in oil well construction we would consider our model appropriate for partially dehydrated gelled drilling fluid, but not for the hard filter cake. In a thermal fouling problem, a continuously baked residual layer will eventually harden. Removal of such hard layers is often not feasible by purely mechanical means, but requires chemical additives and a degree of soaking.

In Allouche *et al.* (2000), and in many geometries with large aspect ratios and/or slow variations in one direction, visco-plastic fluid flows exhibit pseudo-plug behaviour. Typically, this occurs when there is a slow variation in the pseudo-plug velocity, which is a velocity that is computed from an outer expansion. Here pseudo-plugs may occur in the spacer domain for certain geometries, but in the mud wall layer this is thought to be highly unlikely. This is simply because the no-slip condition will assign the plug velocity $w = 0$ for any plug adjacent to the wall.

https://doi.org/10.1017/S0022112003004105 Published online by Cambridge University Press

On the practical side, we have demonstrated that the critical condition of there being no static wall layer depends only on the three dimensionless parameters, n_s, B_s and φ_Y. This contrasts sharply for example with the eight dimensionless groups (at least) needed for a two- or three-dimensional investigation of the static layer thickness in a duct; see for example Allouche *et al.* (2000). Thus, there are considerable advantages to simply attempting to compute the non-existence of static wall layers. Having said this, we must also acknowledge certain dangers in trying to interpret the parametric variations in actual layer thickness by considering variations in maximal layer thickness. As shown in Allouche *et al.* (2000), many parametric variations lead to counter-intuitive variations in actual layer thickness. For the concentric annular solutions with a single static layer, perhaps the result of most interest practically speaking is that the outer layer is generally thicker than the inner layer. For the cementing application that we have focused on, this implies that a static mud layer could exist on the outside of the cemented annulus even when there is no such layer on the inside. Since current ultrasonic cement evaluation techniques generally only detect an inner layer (i.e. on the outside of the casing), this suggests that there will be situations when current evaluation techniques fail.

In our computed results we have focused on geometrically simple examples. Development of the theoretical background needed to consider general shape optimization of functionals such as M_Γ is underway. There are some technical difficulties associated with computing shape derivatives of the yield surfaces. Interestingly, the type of variational inequalities that result from considering the shape derivative of an axial duct flow of a visco-plastic fluid also arise naturally when we consider stopping time selection for visco-plastic BV-diffusion filters; see Frigaard, Ngwa & Scherzer (2002). Other analogies exist with shape optimization for contact/obstacle problems in linear elasticity; see Sokolowski & Zolesio (1991).

The simple example in § 4.1.3 shows that when three-dimensional asymmetries are allowed, even a narrow concentric annulus may not be as simple as it appears. The phenomena of bridging across the gap is an interesting area for further study. As well as a fully numerical approach for such a problem, it would appear that the asymptotic approach to eccentric annular flows of Walton & Bittleston (1991) could be adapted. Some experimental study would also be possible and an apparatus for running annular displacement experiments is under construction at University of British Columbia. Although with a displacement experiment it is not possible to study the maximal layer thickness explicitly, the phenomenon of bridging could be studied. To date the most reliable published experiments on static residual layers are due to Gabard-Cuoq (2001), who has considered displacement of visco-plastic Carbopol solutions by a range of fluids in a circular tube. For those experiments where a static residual wall layer was observed the residual layers appeared to be uniform, but of course bridging has little meaning in a circular tube.

The contribution of I.A.F. has been supported by Schlumberger and NSERC through CRD project 245434, and also by the Pacific Institute for the Mathematical Sciences. The work of S.L. and O.S. has been supported by the Austrian Science Foundation (FWF), grant Y-123INF. The support of our sponsors is gratefully acknowledged. We thank an anonymous referee for bringing to our attention the work of Zwick, Ayyaswamy & Cohen (1996); Huilgol (1998); Huilgol & Nguyen (2001). We also thank Professor C. C. Mei and an anonymous referee for their suggestions on making the results in § 2 more accessible.

https://doi.org/10.1017/S0022112003004105 Published online by Cambridge University Press

Appendix. Proof of Theorem 1

Apart from our extension to multi-fluids, Theorem 1 is analogous to that of Zwick *et al.* (1996), who adapt the earlier work of Yoshioka & Adachi (1971*a*, *b*). Our method of proof is slightly different, and we therefore include the detail below.

Proof. Subtracting (2.1) and (2.2) from (2.18) and (2.19), multiplying by w and integrating over Ω_s and Ω_m gives

$$(\tilde{f} - f)\int_{\Omega} w \,\mathrm{d}\Omega = \int_{\Omega_m} (\tilde{\boldsymbol{\tau}} - \boldsymbol{\tau}_m)\cdot\nabla w \,\mathrm{d}\Omega + \int_{\Omega_s} (\tilde{\boldsymbol{\tau}} - \boldsymbol{\tau}_s)\cdot\nabla w \,\mathrm{d}\Omega, \tag{A 1}$$

where we have used the divergence theorem and the stress continuity conditions repeatedly on each sub-domain. Thus, we have

$$\begin{aligned} F(\boldsymbol{\tau}, f) = F(\tilde{\boldsymbol{\tau}}, \tilde{f}) &- \int_{\Omega_m} (\tilde{\boldsymbol{\tau}} - \boldsymbol{\tau}_m)\cdot\nabla w \,\mathrm{d}\Omega - \int_{\Omega_s} (\tilde{\boldsymbol{\tau}} - \boldsymbol{\tau}_s)\cdot\nabla w \,\mathrm{d}\Omega \\ &+ \int_{\Omega_s} \frac{(|\tilde{\tau} - \tau_{s,Y}| + \tilde{\tau} - \tau_{s,Y})^{1+1/n_s} - (|\tau_s - \tau_{s,Y}| + \tau_s - \tau_{s,Y})^{1+1/n_s}}{(1+1/n_s)\kappa_s^{1/n_s} 2^{1+1/n_s}} \,\mathrm{d}\Omega \\ &+ \int_{\Omega_m} \frac{(|\tilde{\tau} - \tau_{m,Y}| + \tilde{\tau} - \tau_{m,Y})^{1+1/n_m} - (|\tau_m - \tau_{m,Y}| + \tau_m - \tau_{m,Y})^{1+1/n_m}}{(1+1/n_m)\kappa_m^{1/n_m} 2^{1+1/n_m}} \,\mathrm{d}\Omega. \end{aligned} \tag{A 2}$$

We now consider the sign of the integrand in (A 2) at any point in Ω_k and show that there are only positive contributions to $F(\boldsymbol{\tau}, f) - F(\tilde{\boldsymbol{\tau}}, \tilde{f})$. It suffices to consider $|\nabla w| > 0$, since for $|\nabla w| = 0$ we have $\tau_k \leqslant \tau_{k,Y}$ and are left with the term

$$(|\tilde{\tau} - \tau_{k,Y}| + \tilde{\tau} - \tau_{k,Y})^{1+1/n_k} \geqslant 0.$$

Suppose therefore that $|\nabla w| > 0$. From (2.3) we have

$$\nabla w = \frac{(\tau_k - \tau_{k,Y})^{1/n_k}}{\kappa_k^{1/n_k}} \frac{\boldsymbol{\tau}_k}{\tau_k},$$

and we consider the integrand

$$\begin{aligned} I_k = \frac{(|\tilde{\tau} - \tau_{k,Y}| + \tilde{\tau} - \tau_{k,Y})^{1+1/n_k} - (|\tau_k - \tau_{k,Y}| + \tau_k - \tau_{k,Y})^{1+1/n_k}}{(1+1/n_k)\kappa_s^{1/n_k} 2^{1+1/n_k}} \\ - \frac{(\tau_k - \tau_{k,Y})^{1/n_k}}{\kappa_k^{1/n_k}} (\tilde{\boldsymbol{\tau}} - \boldsymbol{\tau}_k)\cdot\frac{\boldsymbol{\tau}_k}{\tau_k} \end{aligned}$$

for the two cases: (i) $\tilde{\tau} > \tau_{k,Y}$, (ii) $\tilde{\tau} \leqslant \tau_{k,Y}$.

Case (i) $\tilde{\tau} > \tau_{k,Y}$: Here, since we have already assumed that $\tau_k > \tau_{k,Y}$, we have

$$\kappa_s^{1/n_k} I_k = \frac{(\tilde{\tau} - \tau_{k,Y})^{1+1/n_k} - (\tau_k - \tau_{k,Y})^{1+1/n_k}}{(1+1/n_k)} - (\tau_k - \tau_{k,Y})^{1/n_k} (\tilde{\boldsymbol{\tau}} - \boldsymbol{\tau}_k)\cdot\frac{\boldsymbol{\tau}_k}{\tau_k}. \tag{A 3}$$

For all $\tilde{\boldsymbol{\tau}}$ of given magnitude (A 3) is minimized when $\tilde{\boldsymbol{\tau}}$ is parallel to $\boldsymbol{\tau}_k$, say $\tilde{\boldsymbol{\tau}} = \lambda\boldsymbol{\tau}_k$. We can also write $\tau_k = \theta\tau_{k,Y}$ for some $\theta > 1$, and since $\tilde{\boldsymbol{\tau}}/\lambda = \boldsymbol{\tau}_k = \theta\tau_{k,Y}$, we have $\theta\lambda > 1$. Using these settings in (A 3) results in

$$\frac{\kappa_s^{1/n_k}}{\tau_{k,Y}^{1+1/n_k}} I_k \geqslant \frac{(\lambda\theta - 1)^{1+1/n_k} - (\theta - 1)^{1+1/n_k}}{(1+1/n_k)} + \theta(\theta - 1)^{1/n_k}(1 - \lambda).$$

The right-hand side is minimized at $\lambda = 1$, giving $I_k \geqslant 0$.

https://doi.org/10.1017/S0022112003004105 Published online by Cambridge University Press

Case (ii) $\tilde{\tau} \leqslant \tau_{k,Y}$: Here we have

$$\kappa_s^{1/n_k} I_k = -\frac{(\tau_k - \tau_{k,Y})^{1+1/n_k}}{(1+1/n_k)} - (\tau_k - \tau_{k,Y})^{1/n_k}(\tilde{\boldsymbol{\tau}} - \boldsymbol{\tau}_k)\cdot\frac{\boldsymbol{\tau}_k}{\tau_k}. \tag{A 4}$$

Again we have $\tau_k = \theta\tau_{k,Y}$ for some $\theta > 1$, and for all $\tilde{\boldsymbol{\tau}}$ of given magnitude, (A 4) is minimized when $\tilde{\boldsymbol{\tau}}$ is parallel to $\boldsymbol{\tau}_k$, say $\tilde{\boldsymbol{\tau}} = \lambda\boldsymbol{\tau}_k$ with $\lambda\theta \leqslant 1$:

$$\begin{aligned}\frac{\kappa_s^{1/n_k}}{\tau_{k,Y}^{1+1/n_k}} I_k &\geqslant -\frac{(\theta-1)^{1+1/n_k}}{(1+1/n_k)} + \theta(\theta-1)^{1/n_k}(1-\lambda),\\ &= \frac{(\theta-1)^{1/n_k}}{(1+1/n_k)}[\theta(1-\lambda)(1+1/n_k) - (\theta-1)]\\ &= \frac{(\theta-1)^{1/n_k}}{(1+1/n_k)}[\theta(1-\lambda)/n_k + (1-\lambda\theta)] > 0.\end{aligned}$$

□

REFERENCES

Allouche, M., Frigaard, I. A. & Sona, G. 2000 Static wall layers in the displacement of two visco-plastic fluids in a plane channel. *J. Fluid Mech.* **424**, 243–277.

Atkinson, K. & Han, W. 2001 *Theoretical Numerical Analysis; a Functional Analysis Framework*. Springer.

Beirute, R. M. 1977 Mechanics of the displacement process of drilling muds by cement slurries using an accurate rheological model. *Soc. Petrol. Engrs Paper* SPE 6801.

Bittleston, S. H., Ferguson, J. & Frigaard, I. A. 2002 Mud removal and cement placement during primary cementing of an oil well; laminar non-Newtonian displacements in an eccentric annular Hele-Shaw cell. *J. Engng Maths* **43**, 229–253.

Changani, S. D., Belmar-Beiny, M. T. & Fryer, P. J. 1997 Engineering and chemical factors associated with fouling and cleaning in milk processing. *Expl Thermal Fluid Sci.* **14**, 392–406.

Couturier, M., Guillot, D., Hendriks, H. & Callet, F. 1990 Design rules and associated spacer properties for optimal mud removal in eccentric annuli. *Soc. Petrol. Engrs Paper* SPE 21594.

Dacoragna, B. 1989 *Direct Methods in the Calculus of Variations*. Springer.

Duvaut, G. & Lions, J. L. 1976 *Inequalities in Mechanics and Physics*. Springer.

Economides, M. J. 1990 Implications of cementing on well performance. In *Well Cementing* (ed. E. B. Nelson), Chap. 1. Schlumberger Educational Services.

Fenie, H. & Frigaard, I. A. 1999 Transient fluid motions in a simplified model for oilfield plug cementing. *Math. Comp. Mod.* **30**(7–8), 71–91.

Frigaard, I. A. 1998 Stratified exchange flows of two Bingham fluids in an inclined slot. *J. Non-Newtonian Fluid Mech.* **78**, 61–87.

Frigaard, I. A. 2001 Super-stable parallel flows of multiple visco-plastic fluids. *J. Non-Newtonian Fluid Mech.* **100**, 49–76.

Frigaard, I. A., Allouche, M. & Gabard-Cuoq, C. 2001 Setting rheological targets for chemical solutions in mud removal and cement slurry design. *Soc. Petrol. Engrs Paper* SPE 64998.

Frigaard, I. A. & Crawshaw, J. 1999 Preventing buoyancy driven flows of two Bingham fluids in a closed pipe; fluid rheology design for oilfield plug cementing. *J. Engng Maths* **36**, 327–348.

Frigaard, I. A., Ngwa, G. & Scherzer, O. 2002 On effective stopping time selection for visco-plastic nonlinear BV diffusion filters. *SIAM J. Appl. Maths* (submitted).

Frigaard, I. A. & Scherzer, O. 1998 Uniaxial exchange flows of two Bingham fluids in a cylindrical duct. *IMA J. Appl. Maths* **61**, 237–266.

Frigaard, I. A. & Scherzer, O. 2000 The effects of yield stress variation on uniaxial exchange flows of two Bingham fluids in a pipe. *SIAM J. Appl. Maths* **60**, 1950–1976.

Frigaard, I. A., Scherzer, O. & Sona, G. 2001 Uniqueness and non-uniqueness in the steady displacement of two viscoplastic fluids. *Z. Angew. Math. Mech.* **81**(2), 99–118.

Gabard-Cuoq, C. 2001 Etude de la stabilité de films liquides sur les parois d'une conduite verticale lors de l'ecoulement de fluides miscibles non-newtoniens. These de l'Universite Pierre et Marie Curie, (PhD thesis), Orsay, France.

https://doi.org/10.1017/S0022112003004105 Published online by Cambridge University Press

Glowinski, R. 1983 *Numerical Methods for Nonlinear Variational Problems*. Springer.

Guillot, D., Hendriks, H., Callet, F. & Vidick, B. 1990 Mud removal. In *Well Cementing* (ed. E. B. Nelson), Chap. 5. Schlumberger Educational Services.

Huilgol, R. R. 1998 Variational principle and variational inequality for a yield stress fluid in the presence of slip. *J. Non-Newtonian Fluid Mech.* **75**, 231–251.

Huilgol, R. R. & Nguyen, Q. D. 2001 Variational principles and variational inequalities for the unsteady flows of a yield stress fluid. *Intl J. Non-Linear Mech.* **36**, 49–67.

Jamot, A. 1974 Déplacement de la boue par le latier de ciment dans l'espace annulaire tubagé-paroi d'un puits. *Revue Assoc. Franc. Techn. Petrol.* **224**, 27–37.

Lockyear, C. F. & Hibbert, A. P. 1989 Integrated primary cementing study defines key factors for field success. *J. Petrol. Tech.* December, 1320–1325.

Lockyear, C. F., Ryan, D. F. & Gunningham, M. M. 1989 Cement channelling: how to predict and prevent. *Soc. Petrol. Engrs Paper* SPE 19865.

McLean, R. H., Manry, C. W. & Whitaker, W. W. 1966 Displacement mechanics in primary cementing. *Soc. Petrol. Engrs Paper* SPE 1488.

Plett, E. A. 1985 Cleaning of fouled surfaces. In *Fouling and Cleaning in Food Processing* (ed. C. Sandu, D. B. Lund & E. A. Plett), pp. 287–311. University of Wisconsin, Madison WI.

Prager, W. 1954 On slow visco-plastic flow. In *Studies in Mathematics and Mechanics*. Academic.

Quarteroni, A., Sacco, R. & Saleri, F. 2000 *Numerical Mathematics*. Springer.

Ravi, K. M. & Beirute, R. M. 1992 Erodability of partially dehydrated gelled drilling fluid and filter cake. *Soc. Petrol. Engrs Paper* SPE 24571.

Smith, D. K. 1987 *Cementing*, Chap. 6, pp. 82–106. Society of Petroleum Engineers.

Sokolowski, J. & Zolesio, J.-P. 1991 *Introduction to Shape Optimisation; Shape Sensitivity Analysis*. Springer.

Szabo, P. & Hassager, O. 1992 Flow of viscoplastic fluids in eccentric annular Geometries. *J. Non-Newtonian Fluid Mech.* **45**, 149–169.

Walton, I. C. & Bittleston, S. H. 1991 The axial flow of a Bingham plastic in a narrow eccentric annulus. *J. Fluid Mech.* **222**, 39–60.

Yoshioka, N. & Adachi, K. 1971*a* On variational principles for a non-Newtonian fluid. *J. Chem. Engng Japan* **4**, 217–220.

Yoshioka, N. & Adachi, K. 1971*b* Applications of the extremum principles for non-Newtonian fluids. *J. Chem. Engng Japan* **4**, 221–226.

Zwick, K. J., Ayyaswamy, P. S. & Cohen, I. M. 1996 Variational analysis of the squeezing flow of a yield stress fluid. *J. Non-Newtonian Fluid Mech.* **63**, 179–199.

https://doi.org/10.1017/S0022112003004105 Published online by Cambridge University Press